

AMERICAN UNIVERSITY OF BEIRUT

TRENDS IN SNOW COVER DYNAMICS OVER THE
LEVANT USING SATELLITE IMAGERY: RESPONSE TO
CLIMATE CHANGE

by
NAJI ANTOINE EL BEYROUTHY

A thesis
submitted in partial fulfillment of the requirements
for the degree of Master of Science
to the Department of Irrigation
of the Faculty of Agriculture and Food Science
at the American University of Beirut

Beirut, Lebanon
January 2020

AMERICAN UNIVERSITY OF BEIRUT

TRENDS IN SNOW COVER DYNAMICS OVER THE
LEVANT USING SATELLITE IMAGERY: RESPONSE TO
CLIMATE CHANGE

by
NAJI ANTOINE EL BEYROUTHY

Approved by:

Dr. Hadi, Jaafar Assistant Professor
Agriculture Science


Advisor

Dr. Issam Bashour, Professor
Agriculture science


Member of Committee

Dr. Ali Chalak, Associate Professor
Agriculture science


Member of Committee

Date of thesis defense: January 27, 2019

AMERICAN UNIVERSITY OF BEIRUT

THESIS, DISSERTATION, PROJECT RELEASE FORM

Student Name: El Beyrouthy Naji Antoine
Last First Middle

Master's Thesis Dissertation Master's Project Doctoral

I authorize the American University of Beirut to: (a) reproduce hard or electronic copies of my thesis, dissertation, or project; (b) include such copies in the archives and digital repositories of the University; and (c) make freely available such copies to third parties for research or educational purposes.


I authorize the American University of Beirut, to: (a) reproduce hard or electronic copies of it; (b) include such copies in the archives and digital repositories of the University; and (c) make freely available such copies to third parties for research or educational purposes

after:

One --- year from the date of submission of my thesis, dissertation, or project.

Two years from the date of submission of my thesis, dissertation, or project.

Three ---- years from the date of submission of my thesis, dissertation, or project.

 20-Feb-2020
Signature Date

ACKNOWLEDGMENTS

Thank you to my advisor Dr. Hadi Jaafar for his continuous support, patience, and immense knowledge. His guidance helped me during my masters. I could not have imagined having a better advisor and mentor.

Thank you to my committee members Dr. Bashour and Dr. Chalak for their precious comments and influence on the thesis.

Thank you to family, my Mother and Father for always believing in me.

Finally, Rachel, who was my backbone every step of the way. You were there when I needed you. Thank you for being you.

Thank you to all who helped accomplish this thesis.

AN ABSTRACT OF THE THESIS OF

Naji Antoine El Beyrouthy for Master of Science
Major: Irrigation

Title: Trends in snow cover dynamics over the Levant using satellite imagery: Response to climate change

Remote sensing is a powerful instrument to monitor snow cover in distant and unreachable areas, where a lot of the precipitation events happening occur as snow. As there is increased pressure on water resources due to climate change, uncontrolled development, and overpopulation, knowledge about the seasonal snow accumulation in the Mediterranean Mountains is vital for the water budget and the region's water management strategies. Snowmelt importance lies in its substantial contribution to the recharge of the karst aquifers supplying water during the dry season, to agriculture as well as domestic and industrial uses in Lebanon. This research consists of a daily, monthly, annual and seasonal remote-sensing based analysis of Albedo, Snow Depth (SD), and a time series analysis of snow cover area (SCA), snow cover days (SCD) of Levant Mountains using Google Earth Engine, between 1985 and 2019. We analyzed MODIS Terra and Aqua daily snow cover product, and all the Landsat archive to generate NDSI for the Levant. The study region covers an area of 28,620 km² and a maximum elevation of 3088m covering Mount and Anti-mount Lebanon. The model analyzes the visible, near-infrared, and shortwave infrared bands, subject to a pixel-based screening process to extract snow extent. The screening process includes a cloud mask, vegetation mask, low reflectance mask, temperature mask, low NDSI, and high SWIR masks. Snow Water Equivalent (SWE) and snow density regressed against remotely sensed and field measurements obtained from literature and regressed against Albedo between 2015-2016 in three different Mediterranean watersheds. Results showed there is a 25-30% decrease in snow cover area, when comparing the means of 1985-2005 and 2005-2019 (2005 year mean change), with a yearly decrease of 12 km² in snow area, representing 1.18 % of the average snow area since 1985 and a non-significant decrease in annual snow cover days by 0.07 day/year since 1985 using Landsat analysis and a significant decrease of the snow cover using the MODIS analysis by about two days/year since 2000. A correlation analysis between snow area and mean annual air temperature and annual precipitation using the ERA5 and the CHIRPS products respectively show that the decrease in snow area is significantly correlated with the temperature increase in the region. No correlation was found between precipitation and snow area. This study contributed to the understanding of the impact of climate change on the temporal variability of water resources in the region and sheds light on the need for climate change adaptation in water resources and irrigation management.

CONTENTS

ACKNOWLEDGMENTS	v
ABSTRACT.....	vi
LIST OF ILLUSTRATIONS	x
LIST OF TABLES	xiii
ABBREVIATIONS	xvi
Chapter	
I. INTRODUCTION	1
II. LITERATURE REVIEW	3
A. Mapping snow using visible and near-infrared products.....	3
1. Mapping snow using the Moderate Resolution Image Spectroradiometer (MODIS).....	4
2. Mapping snow using Landsat	6
B. Mapping snow using microwave products.....	7
C. Snow mapping in complex terrain	9
D. Snow Cover Area (SCA)	10
E. Snow Grain Size retrieval.....	11
F. Snow Water Equivalent retrieval.....	12
G. Field validation/measurements	13

H. Albedo importance and retrieval.....	14
I. Previous research in Lebanon.....	15
J. Google Earth Engine	17
III. MATERIALS AND METHODS	18
A. Study Area	18
B. Snow cover retrieval from MODIS	20
C. Snow cover from Landsat	22
D. Albedo retrieval	24
E. Snow Depth retrieval from Sentinel-1.....	24
F. Correlation of snow area with streamflow	26
G. Correlation of snow area with temperature and precipitation.....	26
H. Trend Analysis and Significance	27
IV. RESULTS AND DISCUSSION.....	29
A. Landsat, MODIS snow detection and snow cover days	29
B. Snow days Trend.....	32
C. Landsat Snow Cover Area	37
D. Landsat Trend Analysis	38
E. MODIS snow cover area	46
F. MODIS Trend Analysis.....	47
G. Snow Density vs. Snow Albedo.....	52

H. Snow Area vs. Temperature vs. Precipitation.....	54
I. Sentinel-1 vs. Field measured snow depth	59
J. River vs. Snow Area.....	60
K. Discussion	62
V. CONCLUSION AND RECOMMENDATIONS.....	64
Appendix	
I. STATISTICAL SIGNIFICANCE.....	64
II. SNOW COVER DAYS.....	70
REFERENCES	72

ILLUSTRATIONS

Figure	Page
1.Spectral signature of different surfaces (USGS, 2016).....	4
2. Study area with basin distribution	19
3. Flow chart of the MODIS Snow detection algorithm also used for Landsat.....	21
4. Comparison between Mid-Season Landsat (left) and MODIS (right) snow detection	30
5. Comparison between Late-Season Landsat (left) and MODIS (right) snow detection	31
6. Landsat and MODIS annual Snow Cover days between 2001 and 2018	32
7. Annual MODIS Snow Cover Days for the whole study area	33
8. Annual Landsat Snow Cover Days for the whole area	33
9. MODIS annual snow cover days over the north, south, east, and west basins.....	34
10. Landsat annual snow cover days over the north, south, east, and west basins	36
11. Annual and Seasonal average Snow Area km ² over the north, south, east, and west areas	38
12. Annual average Snow Area Anomalies km ² over the north, south, east, and west areas	39
13. Annual average Snow Area Anomalies km ² over the north, south, east, and west areas without the 1992 snow season.	40
14. Winter average Snow Area Anomalies km ² over the north, south, east, and west areas	42

15. Spring average Snow Area Anomalies km ² over the north, south, east, and west areas	43
16. Fall average Snow Area Anomalies km ² over the north, south, east, and west areas	44
17. Annual and Seasonal average Snow Area km ² over the north, south, east and west areas	46
18. Annual average Snow Area Anomalies km ² over the north, south, east, and west areas	47
19. Winter average Snow Area Anomalies km ² over the north, south, east, and west areas	48
20. Spring average Snow Area Anomalies km ² over the north, south, east, and west areas	49
21. Fall average Snow Area Anomalies km ² over the north, south, east, and west areas	51
22. Landsat Albedo vs. Field Snow Density observations (Fayad et al., 2017)	53
23. MODIS Albedo vs. Field Snow Density observations (Fayad et al., 2017)	53
24. Annual Average Temperature vs. Annual Snow Area for the North, South, East, West basins	54
25. 5-year moving average for the annual air Temperature °C over the full area between 1985 and 2019.....	55
26. 5-year moving average for the annual precipitation mm over the full area between 1985 and 2019.....	55
27. Comparison between Snow depth retrieved from Sentinel-1 and Snow depth retrieved from an Automatic weather station's Acoustic sensor between 2015 and 2016 (Fayad et al., 2017)	59

28. Seasonal Snow Area vs. Streamflow for the Litany river at Jib Jannine.....	60
29. Annual precipitation mm over the Litani watershed between 1985 and 2019	61

TABLES

Table	Page
1. Wavelength and Resolution of available Landsat 4-5-7-8 bands	7
2. Basin area in km ²	20
3. Weighing coefficients for Landsat 4,5,7,8 albedo calculation	24
4. Trend analysis and Significance Tests	28
5. MODIS trend results for the annual snow cover days over the north, east, west, and south basins.....	35
6. Landsat trend results for the annual snow cover days over the whole area, north, east, west, and south basins.....	37
7. Landsat annual trend results for the snow cover area anomalies over the north, east, west, and south basins.....	41
8. Landsat seasonal trend results for the snow cover area anomalies over the north, east, west, and south basins.....	45
9. MODIS seasonal trend results for the snow cover area anomalies over the north, east, west, and south basins.....	50
10. Snow Area % mean Change for the North, South, West, East and the whole Lebanese area using the Landsat dataset between 1985 and 2019 snow seasons.....	52
11. Results of correlation analysis between Annual Temperature and Annual snow Area	57
12. Results of correlation analysis between Seasonal Temperature and Seasonal snow Area (All Seasons).....	57

13. Results of correlation analysis between the Winter Temperature and Winter snow Area.....	57
14. Results of correlation analysis between the Spring Temperature and Spring snow Area.....	58
15. Results of correlation analysis between the Fall Temperature and Fall snow Area .	58
16. Statistical significance of the 5-year moving average annual air Temperature trend analysis.....	58
17. Significance of the monthly and seasonal Litani Flow vs. Snow Area	61
18. Upper Litani Flow (Mm ³), Snow Area (Km ²), and Precipitation (mm) 2005 year mean change and % change	61
19. Statistical results for the Annual Landsat 5-year moving average Snow Area for all basins	64
20. Statistical results for the Winter Landsat 5-year moving average Snow Area for all basins	65
21. Statistical results for the Spring Landsat 5-year moving average Snow Area for all basins	65
22. Statistical results for the Summer Landsat 5-year moving average Snow Area for all basins	66
23. Statistical results for the Fall Landsat 5-year moving average Snow Area for all basins	66
24. Statistical results for the Annual MODIS 5-year moving average Snow Area for all basins	67
25. Statistical results for the winter MODIS 5-year moving average Snow Area for all basins	67

26. Statistical results for the spring MODIS 5-year moving average Snow Area for all basins	68
27. Statistical results for the summer MODIS 5-year moving average Snow Area for all basins	68
28. Statistical results for the fall MODIS 5-year moving average Snow Area for all basins	69
29. MODIS annual snow cover days	70
30. Landsat annual snow cover days	71

ABBREVIATIONS

w_b	Band Specific Weighing number
°	Degrees
μm	Micrometer
%	Percent
σ_{vh}^0	Polarization of the Sentinel 1 VH band
σ_{vv}^0	Polarization of the Sentinel 1 VV band
pred	Red Band Reflectance
ρ	Reflectance
ρ_{SWIR}	Short Wave Infrared Reflectance
3D	Three Dimensional
2D	Two Dimensional
a.s.l.	Above Mean Sea Level
AMSR-E	Advanced Microwave Scanning Radiometer - Earth Observing System
AVHRR	Advanced Very High-Resolution Radiometer
AVIRIS	Airborne Visible/Infrared Imaging Spectrometer
API	Application Program Interface
AWS	Automated Weather Station
DJF	December, January, February
dB	Decibel
C°	Degrees Celsius
ESA	European Space Agency
FC	Evergreen Forest Cover Fraction

GHz	Gigahertz
GEE	Google Earth Engine
IMS	Interactive Multisensor Snow and Ice Mapping System
JJA	June, July, August
K	Kelvin
Km	Kilometer
Km ²	Kilometers Square
L8	Landsat Eight
L5	Landsat Five
L4	Landsat Four
L7	Landsat Seven
Lat	latitude
LIDAR	Light Detection and Ranging
Lon	Longitude
MAM	March, April, May
Max	Maximum
m	Meter
Min	Minimum
MODIS	Moderate Resolution Image Spectroradiometer
MYD10A1	MODIS Aqua Daily Snow Cover Map
MYD	MODIS Aqua Sensor
MODSCAG	MODIS Snow Covered Area and Grain-size
MOD10A1	MODIS Terra Daily Snow Cover Map
MOD	MODIS Terra Sensor

MSS	Multispectral Scanner System
NASA	National Aeronautics and Space Administration
NESDIS	National Environmental Satellite, Data, and Information Service
NOAA	National Oceanic and Atmospheric Administration
NWS	National Weather Surface
NDSI	Normalized Difference Snow Index
NDVI	Normalized Difference Vegetation Index
RADAR SAT	Radar Satellite
SMMR	Scanning Multichannel Microwave Radiometer
SC	Scow Cover presence
SON	September, October, November
SWIR	Short Wave Infra-Red
SCA	Snow Cover Area
SD	Snow Depth in meters
SNODIS	Snow Distribution
SI	Snow Index
SWE	Snow Water Equivalent
SMM/I	Special Sensor Microwave/Imager
St.	Standard
SAR	Synthetic Aperture Radar
Tb	Temperature band
TM	Thematic Mapper
V5	Version 5
V6	Version 6

CHAPTER I

INTRODUCTION

Snow plays an essential role in the Earth's radiation balance. Analyzing snow cover can indicate the impacts of climate change. Snow cover area (SCA) and Snow water equivalent (SWE) are fundamental in our understanding of snow hydrology. Higher air temperatures cause elevated snow lines and an increase in rainfall at the expense of snow accumulation in several parts of the world (Knowles, Dettinger, & Cayan, 2006). Snow is an essential contributor to the hydrologic cycle, especially in mountainous areas, as the seasonal snow cover is a significant factor in a region's freshwater supply (Jeff Dozier, Bair, & Davis, 2016). While breakthroughs took place with SCA estimation and validation, SWE remains the hardest and most crucial hurdle with snow hydrology, especially in the areas that lack sufficient and reliable ground measurements (Fayad, Gascoin, Faour, López-Moreno, et al., 2017). Remote sensing can help distinguish snow from other terrestrial objects by taking advantage of the snow's interaction with the electromagnetic spectrum. This interaction is utilized by either active or passive techniques using either the visible and infrared or the microwave part of the electromagnetic spectrum (Foster, Hall, Kelly, & Chiu, 2009; Frei et al., 2012; Hüsler, Jonas, Riffler, Musial, & Wunderle, 2014). The use of remote sensing for snow detection is hindered by several factors: cloud cover, topography, and forest cover.

Renewable water resources for Lebanon are estimated at 2.7 billion cubic meters for an average water year divided between 2.2 billion cubic meters as surface water and

0.5 billion cubic meters as groundwater (MOEW, 2010). Precipitation varies over the years. Between 30 % and 40 % of the annual precipitation falls as snow (Shaban, Faour, Khawlie, & Abdallah, 2004). On average, SWE contributes to 26% of the national hydrologic cycle (Mhawej, Faour, Fayad, & Shaban, 2014). The importance of snowmelt as a significant source of freshwater is shown in a study done by (Margane et al., 2013), which estimated that snowmelt contributed to up to 81% of the groundwater recharge for the Nahr el Kalb basin, which alone contributes up to 75% of Beirut's potable water from Jeita's karstic spring replenished by snowmelt (Margane et al., 2013). As a Mediterranean climate characterizes Lebanon, this makes it particularly vulnerable to climate change (Giorgi & Lionello, 2008; Morán-Tejeda, Lorenzo-Lacruz, López-Moreno, Rahman, & Beniston, 2014), which has been witnessed by the dry periods during the past two decades (Cook, Anchukaitis, Touchan, Meko, & Cook, 2016) with above-average temperatures and below-average precipitation (Kelley, Mohtadi, Cane, Seager, & Kushnir, 2015). Future projections indicate a shift of Mediterranean mountain basins moving from snow to a rain dominated regime (Goulden & Bales, 2014; Maurer, Stewart, Bonfils, Duffy, & Cayan, 2007). Since Lebanese mountains fall in this category, it is expected by 2040 and with a rise of 2°C to reduce snow depth by 50% around 2000 m a.s.l., and snow seasons to be shorter by 2 to 6 weeks (MOEW, 2010). The objective of this research is to retrieve and analyze snow cover area for the past 35 years over the Levant and comparing it with temperature and precipitation trends, which will show the effect of climate change on snow cover, and subsequently a decrease of the available ground and surface water.

CHAPTER II

LITERATURE REVIEW

In this chapter, we will discuss previous work about snow hydrology, mapping of snow extent, depth, and snow water equivalent (SWE) estimations retrieved via field measurements, multispectral and passive microwave sensors, and snowmelt runoff models for retroactive SWE estimation. Several products are available for remote sensing observations. The most widely used for climate observations are the Moderate Resolution Image Spectroradiometer (MODIS) and Landsat.

We will proceed by dividing these products into two groups, taking into consideration the method of data retrieval, whether by using the visible and near-infrared or the microwave part of the electromagnetic spectrum, explaining their importance and showing previous studies about each product.

A. Mapping snow using visible and near-infrared products

The presence of snow and the snow extent are easily observable due to the high reflectance of snow and albedo (around 80% for old snow and close to 90% for fresh snow) (Dietz, Kuenzer, Gessner, & Dech, 2012). Problems arise when images have cloud cover or are inefficiently illuminated. Cloud cover has similar albedo to snow but can be distinguished using near infra-red (as snow has low reflectance for near infra-red while clouds have a high reflectance) (Figure 1).

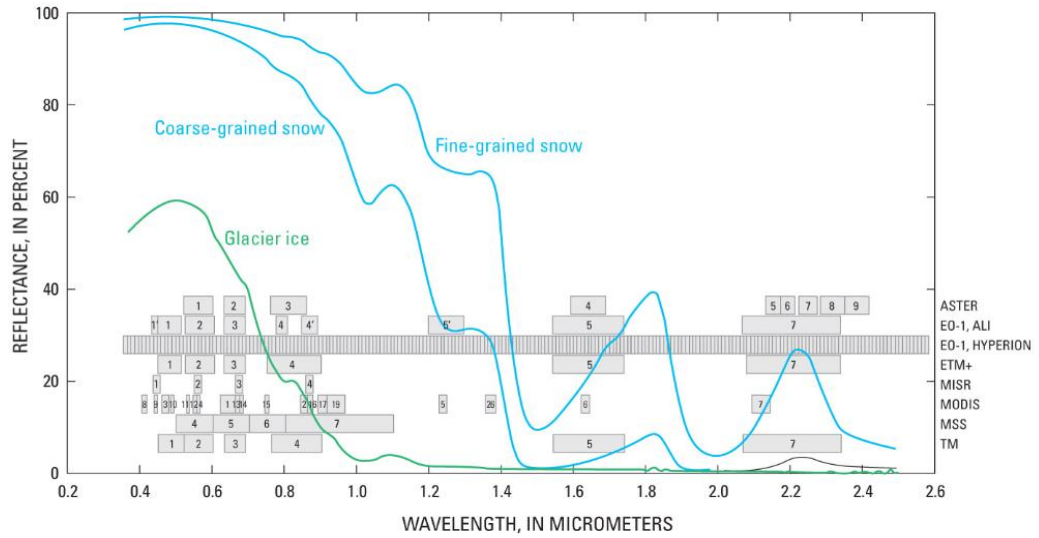


Figure 1. Spectral signature of different surfaces (USGS, 2016)

1. Mapping snow using the Moderate Resolution Image Spectroradiometer (MODIS)

MODIS snow products have been used and validated on a regional and global scale. The sensor captures radiation in 36 spectral bands ranging from 0.4 μm to 1.4 μm incorporating the visible, near-infrared, and infrared parts of the electromagnetic spectrum. MODIS snow cover products used in this research (MOD10A1 and MYD10A1) consist of daily gridded snow cover and albedo derived from radiance data available since 2000 at 500 m spatial resolution using a fully automated algorithm that includes cloud detection. Hall, (2002) showed that the MODIS snow-cover maps compare favorably with current operational maps, and perform better than passive microwave-derived snow-cover maps during the daytime and in the early and late months in the Northern Hemisphere when the snow is wet. The MODIS Normalized Difference Snow Index is used to map snow cover between band 4 (5.45-5.56 μm) and band 6 (1.628-1.652 μm), NDSI is designed to detect snow cover across the entire range of values from 0.1 - 1.0. The range used is the theoretical range of snow, which allows

every individual to set a certain threshold of snow detection rather than being restricted to 0.4 – 1 (Hall et al., 2002). MODIS products are always being improved, with the latest product that improved on the binary snow map from the V5 to the V6 with an NDSI snow cover that ranges from 0 or no snow cover to 100 or full snow cover. These changes provide higher flexibility for greater accuracy. Once NDSI has been calculated, it goes through many spectral threshold tests to identify whether the pixel identified as snow is snow. This threshold is changed in forested areas depending on both the NDSI and Normalized Difference Vegetation Index (NDVI). After the threshold has been defined, the low reflectance pixels, being less than or equal to 0.1 in MODIS band two and less or equal to 0.11 in Band 4, are set to no-decision. Pixels having an NDSI between 0 and 0.1 are reversed to no snow. Pixels that appeared as snow but were too warm are also reversed to no snow, where MODIS band 31 Tb (brightness temperature) is used, as any pixel below 1300 m and having a Tb higher or equal to 281K are reversed to no snow, and everything above 1300 is set to unusually warm snow. A Short-Wave Infrared (SWIR) reflectance threshold was set and served two purposes. First, preventing non-snow features that appear similar to snow from being detected as snow; and second, allowing snow to be detected where snow-cover SWIR is anomalously high. Snow SWIR is typically less than 0.2. The SWIR reflectance screen thus utilizes two thresholds, where snow pixel having a SWIR higher than 0.45 are classified as no snow, and the pixel that had a SWIR between 0.2 and 0.45 are classified as unusually high for snow. Lake ice is flagged so that the user can decide to mask or extract them (Hall et al., 2002). NASA provides a grading system for their snow products between level 2 and level 3 for a variety of uses. These include a daily and

eight-day composite level 2 swath product. Level 3 products available on a 10° lat/lon tile, in addition to a daily, 8-day, and monthly mapped at a 0.05° resolution.

2. Mapping snow using Landsat

Previous work on mapping snow cover consisted of using the Landsat Multispectral Scanner System (MSS) (Lichtenegger, Seidel, Keller, & Haefner, 1981; Staenz & Haefner, 1981), which was the precursor to the Thematic Mapper (TM) (Bourdelles & Fily, 1993; Jeff Dozier, 1989; Fily, Bourdelles, Dedieu, & Sergent, 1997; Rosenthal & Dozier, 1996; Selkowitz & Forster, 2016). The first 5 Landsats carried the MSS, it had four bands between the visible and the near-infrared portion of the electromagnetic spectrum, with the addition of a fifth band on Landsat 3 that responds to thermal (heat) infrared radiation. The Thematic Mapper (TM) that started with Landsat 4 is an advanced, multispectral scanning, Earth resources sensor designed to achieve higher image resolution, sharper spectral separation, improved geometric fidelity and greater radiometric accuracy and resolution than the MSS sensor. Jeff Dozier, (1989) used the Landsat thematic mapper for cloud/snow discrimination and found that cloud detection can easily be done between 1.55 μm and 1.75 μm where reflectance of the clouds is greater than snow. The Enhanced Thematic Mapper was introduced with the Landsat 7 (Selkowitz & Forster, 2016; Vogel, 2002). While the previous satellites carried only two sensors, the Thermal Infrared Sensor was added to the Landsat 8 satellite, which added upon the existing bands two long-wave infrared bands (Table 1).

Table 1. Wavelength and Resolution of available Landsat 4-5-7-8 bands

Bands	Landsat 4-5 Wavelength (micrometers)	Landsat 4-5 Resolution (meters)	Landsat 7 Wavelength (micrometers)	Landsat 7 Resolution (meters)	Landsat 8 Wavelength (micrometers)	Landsat 8 Resolution (meters)
Coastal	-	-	-	-	0.435 - 0.451	30
Blue	0.45 - 0.52	30	0.45 - 0.52	30	0.452 - 0.512	30
Green	0.52 - 0.60	30	0.52 - 0.60	30	0.533 - 0.590	30
Red	0.63 - 0.69	30	0.63 - 0.69	30	0.636 - 0.673	30
NIR	0.76 - 0.90	30	0.77 - 0.90	30	0.851 - 0.879	30
SWIR1	1.55 - 1.75	30	1.55 - 1.75	30	1.566 - 1.651	30
SWIR2	2.08 - 2.35	30	2.09 - 2.35	30	2.107 - 2.294	30
Thermal 1	10.40 - 12.50	120*(30)	10.40 - 12.50	60*(30)	10.60 - 11.19	100*(30)
Thermal 2	-	-	-	-	11.50 - 12.51	100*(30)
Panchromatic	-	-	0.52 - 0.90	15	0.503 - 0.676	15
Cirrus	-	-	-	-	1.363 - 1.384	30

original band resolution*(resampled resolution)

B. Mapping snow using microwave products

Snow is efficient at scattering the natural radiation emitted by the earth, due to the similarity between the snow grain size and the microwave wavelength. Consequently, it is relatively easy to distinguish between snow and non-snow surfaces due to the diminishing emissions for the snowy surface (Scherer et al., 2005). Jeff Dozier et al., (2016) showed that passive microwave sensors provide good information on thin, cold snow in areas of simple topography but suffer in mountain terrain and generally underestimate the SWE. Additionally, under perfect conditions, the amount of microwave scattering is proportional to the number of snow grains in a snowpack, which makes it a great tool in estimating the Snow Water Equivalent (Frei et al., 2012). Furthermore, microwave remote sensing is unaffected by non-precipitation clouds and does not require the presence of sunlight contrary to the visible and infra-red techniques (Chang, Foster, & Hall, 1987; Chris Derksen, 2008; C Derksen, Walker, & Goodison, 2005). Some limitations arise when using microwave radiation to detect snow cover,

especially with the presence of liquid water, due to rain on snow events or snowmelt. Furthermore, the microwave sensor's footprint must be large (around 25 Km) because of the weak microwave signals emitted by the earth (Frei et al., 2012).

Microwave products have been available since 1978 with the Scanning Multichannel Microwave Radiometer (SMMR) till 1987 followed by Special Sensor Microwave/Imager (SSM/I) since 1987 with The Advanced Microwave scanning radiometer – earth observation (AMSR-E) being introduced in 2002 and served till 2011 (Srivastava, Pandey, Suman, Gupta, & Islam, 2016). AMSR-E was developed by the Japan Aerospace Exploration Agency improving on SMMR and SSM/I, measuring geophysical variables including precipitation rate, water vapor, sea surface winds, sea surface temperature, sea ice concentration, snow water equivalent, and soil moisture. AMSR-E system had twelve channels, with six frequencies. It measured horizontal and vertical polarized brightness temperature. Spatial resolution varies between 5.4 and 56 km, depending on the frequency (Srivastava et al., 2016). The AMSR-E algorithm for SWE estimation uses channels that were previously unavailable for SSM/I and SMMR. Snow depth is derived from a mixture of microwave brightness temperature at different frequencies weighted by the difference between vertical and horizontal frequencies (Srivastava et al., 2016).

One of the latest microwave missions in effect is the Sentinel-1 mission, which started on the 3rd of April 2014, comprises of a constellation of two polar-orbiting satellites, operating day and night performing C-band synthetic aperture radar imaging, enabling them to acquire imagery regardless of the weather (Lievens et al., 2019). Besides the use of microwave imagery for snow area estimation, Sentinel 1 has been used for snow depth measurements. Accurate snow depth estimations are very

important in terms of snow observations, especially for snow water equivalent estimations. Previous studies were limited to backscatter measurements in copolarization, and measurement on shallow snow. Which lead to the early satellite measurements having low sensitivity and only used for monitoring snow presence or absence. Lievens et al., (2019) demonstrated the use of Sentinel-1 backscatter σ in copolarization VV and cross-polarization VH retrieved from the ESA Sentinel 1A and 1B for snow depth estimation across the northern hemisphere, which showed good results when compared to field data measured using a scatterometer over a large area in Michigan where an increase in σ_{vh}^0 coincided with the increase of the snow depth. However, over the Swiss Alps, the results showed a negative relationship where an increase in σ_{vh}^0 coincided with an increase of snow depth, the negative relationship can occur in a situation where the attenuation of ground scattering by the snowpack is stronger than the scattering contribution from the snowpack. For future improvements, it is recommended to study the effect of snow wetness using tower-mounted radar on $\sigma_{vh}^0/\sigma_{vv}^0$. At the moment, Sentinel 1 is the only SAR mission providing high-resolution backscatter measurements at the C band 5.4 GHz with a 6-day latency (Lievens et al., 2019).

C. Snow mapping in complex terrain

One of the main hurdles facing remote sensing in general and snow in particular, is the effect of complex terrain on retrieving reliable and accurate data, as the influence of slope, land cover, solar illumination, and aspect will alter the reflectance characteristics of the image. Jeff Dozier, (1989) showed the significance of the illumination angle on snow detection, which was corrected by using the slope and the

local solar illumination angle. Rugged terrain surfaces are illuminated not only by the direct solar irradiance but also by the reflected irradiance from the surface around them, where, in some cases, snow in the shadow will be darker than vegetation and rocks in the light, which can be solved by simple band thresholds. Accordingly, the MODSCAG model was introduced to estimate mean grain size and fractional snow cover and albedo from MODIS (MOD09GA), using a linear spectral mixture with a library of endmembers consisting of the reflectance characteristics of different surfaces (Painter et al., 2009). Liu et al., (2008) showed that fractional snow cover area retrievals by MODSCAG decrease over forest canopies with increasing view zenith angle.

Other studies focused on artificial neural networks technics by training using surface stations observations. Unfortunately, this is limited by the density and the number of stations available for training in the study area (Tong, Déry, Jackson, & Derksen, 2010).

D. Snow Cover Area (SCA)

Early 1980s snow cover analysis focused on the mapping of snow extent with multispectral sensors such as Landsat Multispectral Scanning Subsystem (MSS), Landsat Thematic Mapper (TM) and the Advanced Very High-Resolution Radiometer (AVHRR). Before that, snow maps were produced by trained meteorologists, who would manually produce the images by visually analyzing photographs, reproduce it and then digitize it at a resolution of 150 to 200 km (Frei et al., 2012).

Jeff Dozier, (1989) proposed the use of a snow index based on the normalized band difference for mapping snow cover and qualitatively reporting grain size. The

index focused on binary classifying each pixel with snow or no snow, which showed good results for discriminating snow from other surfaces like lake ice and clouds. The normalized difference snow index is still in use today.

E. Snow Grain Size retrieval

Snow grain size estimation is an important parameter, as it directly affects the density and albedo of the snowpack and provides knowledge about the age of the snow cover as fresh snow tends to have small grain size, retrieval of snow grain size from AVHRR, Landsat TM has already been done qualitatively by Leroux, (1998) which showed that simulations based on the spherical representation of snow grains were not able to reproduce either the observed bidirectional reflectance or the observed polarized bidirectional reflectance at all the view angles (Fily et al., 1997). J Dozier, (1987) showed that it is possible to map snow grain size by using the Landsat bands 4 and 5 spanning between 0.76-0.9 μm and 1.55-1.75 μm respectively, but this method has its limits where if the grain size is higher than 250 μm the reflectance for band five will drop to 0%, but all the methods relied on the fact that the pixel tested had a 100% snow cover. While other methods for snow grain size were hindered by liquid water content in the snowpack, Painter used AVIRIS, which allowed them to overcome the uncertainty that plague the previous methods (Painter, Dozier, Roberts, Davis, & Green, 2003).

F. Snow Water Equivalent retrieval

Snow Water Equivalent (SWE) is one of the most if not the most crucial parameters in snow hydrology as it is an assessment of the water resource available, and like any method used for SWE estimation requires validation. With enough resources that could be done on a small basin but applying it to a large area seems impractical without the advantage that remote sensing brings. Jonas, Marty, & Magnusson, (2009) estimated snow water equivalent using four parameters: season, snow depth, site altitude, and snow-climate region. These parameters were used to derive snow bulk density applicable to the seasonal snow in the Swiss Alps and similar areas. Jeff Dozier et al., (2016) discussed the different other methods of estimating the snow water equivalence like retroactive reconstruction which will be discussed later, interpolation with surface networks which do not cover the elevated areas and do not account for slope variability, Passive microwave sensors provide useful information on areas of simple topography but suffer in mountains terrain and generally underestimate the SWE, and current weather models are too coarse to simulate multiple snow events. Another method used for SWE estimation relies on retroactive reconstruction, using backward calculations of snowmelt. The only disadvantage is that this method only works one way, as it can only be used when all the snow has melted, and will only go back to the last snowfall event and cannot be applied for estimation during another snow season. One of the models for SWE estimations retroactively is SNODIS. This model uses the duration of snow cover, to backward calculate the peak SWE and the snowmelt for the season. Cline, Elder, & Bales, (1998) showed that SNODIS presented strong indication of SWE distribution and snowmelt estimation over a regional scale.

Small basins become a concern, especially with harsh topography, and the large spatial resolution.

G. Field validation/measurements

Validating data is crucial, but sometimes that may include some inherent difficulties. These difficulties include validation by comparing spatially generated imagery to point measurements, especially in unreachable or sparse station network areas. Unfortunately, this is typical to high altitude areas where snow is most prevalent (Chang et al., 2005).

Apart from the use of Automated Weather Stations for snow depth, snow pillows have been used for SWE estimation. Snow pillows are envelopes of stainless steel or synthetic rubber containing an antifreeze solution. As falling snow accumulates on the pillows, it exerts pressure on the antifreeze solution. The calibrated sensors will read the exerted pressure and calculate the weight of the overlying snow. The weight of the snow can be used to calculate the snow water equivalent. Even though they are in some situations affected by bridging of the frozen layers inside the snow, which will affect the SWE readings, they are still the standard ground-based method for SWE measurement. Since this is a point measurement of SWE, problems arise when trying to interpolate the snow cover between the snow pillows and whether this is representative of the on-field conditions, where most of the meteorological sites lie on nearly flat terrain due to the difficulty with reaching rough terrain, and snow pillow's limited ability to be deployed with ease. In contrast to sloped terrain, as the snow season ends and all that's left is the ephemeral/patchy cover where snowpacks will remain on flat

surfaces but will melt off the sloped surfaces facing the sun leaving them bare. To solve this issue, remotely sensed data are used to fill the gaps and weigh in on the interpolation, whether it is 2D or 3D data (Hill et al., 2019).

Similar problems arise when using snow coring devices for snow depth and SWE measurements. The insertion of the device can cause compaction, and the failure to extract it properly may cause the snow to fall out of the core. Generally, 10% accuracy in snow depth and density readings is used (Hill et al., 2019).

On the other hand, depth is one of the easiest parameters to read for snow monitoring, it can easily be done with a graduated device, or automatically be done using an acoustic sensor mounted on an automated weather station. Similarly, reliable remote sensing of snow depth can be done by airborne observation stations using LIDAR, which can be expensive, on a limited area, and a limited revisit time (Hill et al., 2019).

H. Albedo importance and retrieval

The albedo of the snow surface is one of the most straightforward surface properties measured by remote sensing. Albedo is defined as the portion of the reflected to the incoming solar radiation. The surface reflectivity depends on snow properties such as water content, snow depth, grain size and shape, presence of impurities (Akyürek & Tekeli, 2006). The decreased reflectivity is attributed to impurities in the snowpack due to melting and refreezing (Painter et al., 2009), presence of dust, pollen, and aerosols (Frei et al., 2012). Given the lack of in-situ observations, many studies have used optical remote sensing for snow albedo retrieval (Deems, Painter, &

Finnegan, 2013; Jeff Dozier & Painter, 2004; Frei et al., 2012; Seidel & Martinec, 2004).

The precision of albedo retrieval using remote sensing has been proved In the Armenian Plateau; the MOD10A1 albedo was found to be consistent with in situ measurements in terms of magnitude and temporal variability, with a small positive bias due to differences in the acquisition time (Akyürek & Tekeli, 2006). In some other cases, due to the rough topography, the coarse-resolution albedo products from MODIS underestimated the in-situ snow albedo due to the late-season ephemeral snow patches in a MODIS pixel, especially during the melting periods.

I. Previous research in Lebanon

Previous studies in the region consisted of a combination of field and remotely sensed measurements to determine snow characteristics. Mhawej et al., (2014) studied the use of MODIS Terra and Aqua data to retrieve snow area at a 500-meter resolution and ASMR-E for SWE measurements at 25 Km resolution between 2002 and 2012. These products were combined for SWE retrieval at a subpixel level. The correlation between the volumes and spatial extent of snow in function of altitude was evaluated. The results showed a great correlation between the snow area and SWE. The combination of both instruments was found to be practical in the derivation of sub-pixel SWE at 500 m spatial resolution.

Fayad et al., (2017) provided the first dataset of snow and meteorological conditions in Mount Lebanon which was used in this research. The observation network became fully operational in 2014 with three automated weather stations in three

different watersheds. Providing mean and seasonal snow properties during the 2014-2015 and the 2015-2016 snow seasons, the results showed that SWE peaks around mid-March in elevated areas, while peaking around mid-February at low and mid-latitude areas, for the peak SWE values, 103 and 83 cm water equivalent for CED, 127 and 158 cm water equivalent for MZA, and 59 and 36 cm water available for LAQ between the 2014-2015 and 2015-2016 seasons respectively from the automatic weather denoted by MZA for the Mzar station, the LAQ for the Laqlouq station and the CED for the cedars station located in the Kelb, Ibrahim, Abou Ali watersheds respectively. The average snow density for the three watersheds ranged between 440 and 489 kg/m³ for the two seasons.

Another study was done by Aouad-Rizk et al., (2005) was restricted to the Nahr el Kalb basin. This research consisted of studying the physical characteristics of snow, which include snow cover distribution, snowmelt and apparent density of snow to design an empirical snowmelt model based on the evolution of energy balance with time, which was used to determine the SWE for the area retroactively. Aouad-Rizk found that the apparent density of fresh snow in Lebanon is always greater than 0.25 kg dm⁻³ for altitudes below 2200 m, and greater than 0.18 kg dm⁻³ above 2200 m, the shape of snow is spherical and hail-like (1–6 mm), below 1800 m, then irregular grains (0.5–3 mm) from 1800 to 2300 m, the snow covering Mount Lebanon frequently covers a surface of 2000 km², i.e., 20% of the total area of the country. The corresponding quantity of water stored if the snow covers only 1600 km² is 1.1×10^9 m³. Such a quantity of water was held in snow cover over Mount Lebanon for three months in 2001.

Shaban et al., (2004) studied the melting behavior of snow on Mount-Lebanon. Backed up by field measurements, they used remote sensing to classify the area covered by snow into five snow melt potential zones, as well as proving that snow depth and snow/water ratio are directly proportional to altitude and snow coverage while being inversely proportional to the slope angle.

J. Google Earth Engine

Google Earth Engine is a catalog of satellite imagery and geospatial datasets with planetary-scale analysis capabilities. It is freely available to detect, map, and quantify changes and trends on the Earth's surface. It is accessed and controlled through an Internet-accessible application programming interface (API) that enables rapid analysis and visualization of results (Gorelick et al., 2017).

CHAPTER III

MATERIALS AND METHODS

We describe the retrieval of SCA and SWE using surface reflectance from MODIS, NASA's moderate resolution imaging spectroradiometer, Landsat Multispectral Scanning Subsystem (MSS), Landsat Thematic Mapper (TM), and Sentinel-1.

A. Study Area

This study focuses on the Mount- and Anti-Lebanese mountain regions covering an area of 28,619.46 km², including Lebanon and Syria. The elevation ranges between 0 and 3088 meters above mean sea level. The climate is Mediterranean, where most precipitation falls during the winter season between December and March. The average annual precipitation is around 705 mm (Jaafar, Ahmad, Holtmeier, & King-Okumu, 2019).

The region has been divided into nine basins based on the SRTM 30 meter DEM (Figure 2). The western slopes of Mount Lebanon, affected by orographic precipitation, has been divided into two basins. The northern basin named WestNorthWest includes the Kabir, Oustuene, Barid-Arka, AboAli, Jouz, Ibrahim watersheds, and the southern basin named WestSouthWest includes the Kalb, Beirut, Damour, Awali, Zahrani-Sinic watersheds. The Bekaa valley was divided into four basins named EastNorthWest, WestNorthEast, EastSouthWest, WestSouthEast using the highest points between the Litani and Orontous watersheds as a Northern and Southern divide for the valley and

the river path as the divide between eastern and western basins. The Hasbani river was given its basin named SouthSouthEast. The eastern slopes of the Lebanon Mountains were divided into northern and southern named EastNorthEast and EastSouthEast. The area for each basin is shown in (Table 2).

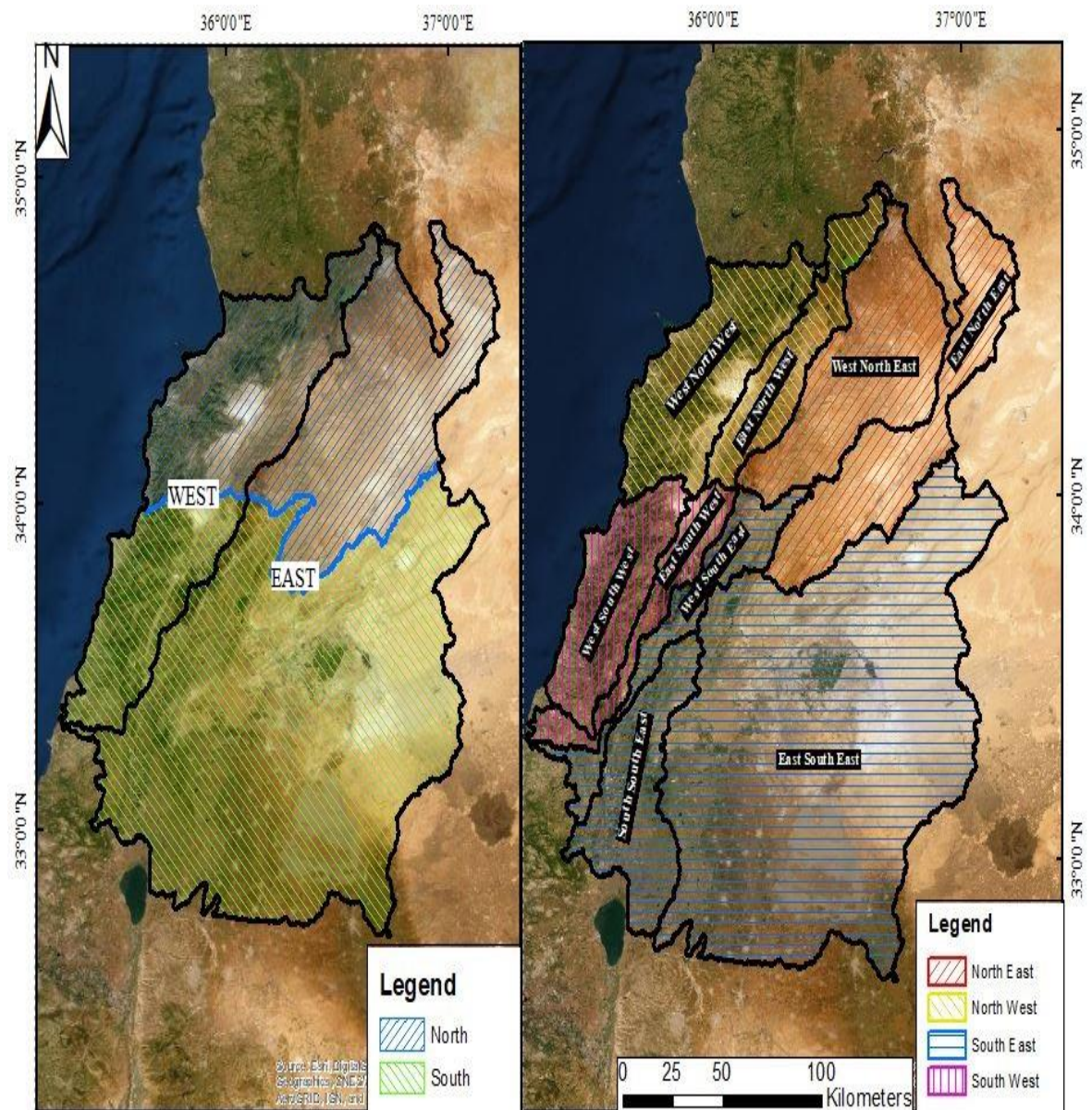


Figure 2. Study area with basin distribution

Table 2. Basin area in km²

Basins	ESE	ENE	WSE	WNE	ESW	ENW	WNW	WSW	SSE
Area (km ²)	12554.12	2751.30	1302.46	3028.39	1025.89	1507.02	2614.52	1818.06	2017.82

B. Snow cover retrieval from MODIS

All the MODIS images that are available from 24-2-2000 for Terra (MOD), 04-07-2002 for Aqua (MYD) were used. Both Terra and Aqua images were used as there is 3 hours of lag between both images. This gap allowed us to choose the Aqua image in case the Terra image was cloudy and vis-versa. The first step consisted of checking each Terra image. If it was clear, then it would be directly used. If the Terra image was cloudy, the clear Aqua image would be used. If the Terra and Aqua images were partly cloudy, a mosaic would be produced from the clear parts of each image and used. All of the images were analyzed and classified. In the case of a significant snow event, where heavy cloud cover would be obstructing snow extent analysis for a few days in a row, daily precipitation would be analyzed to determine the highest rainfall day and this day would be used as an anchor having the peak snow area by using the lowest snow line for each watershed and assuming that the area above that line would be covered with snow. A Cubic interpolation was used between the peak cloudy snow cover day and the nearest clear day.

Since the MODIS MOD10A1 and MYD10A1 are available with a snow cover band, snow area retrieval is straight forward and does not need further restrictions (Figure 3). After setting a threshold on the NDSI Snow Cover band from MOD10A1 and MYD10A1, the next step consisted of making each pixel into a binary product where “1” means the presence of snow cover and 0 means absence. After running this

algorithm on all the images, the area was calculated, summed for the whole image, and plotted in a time series.

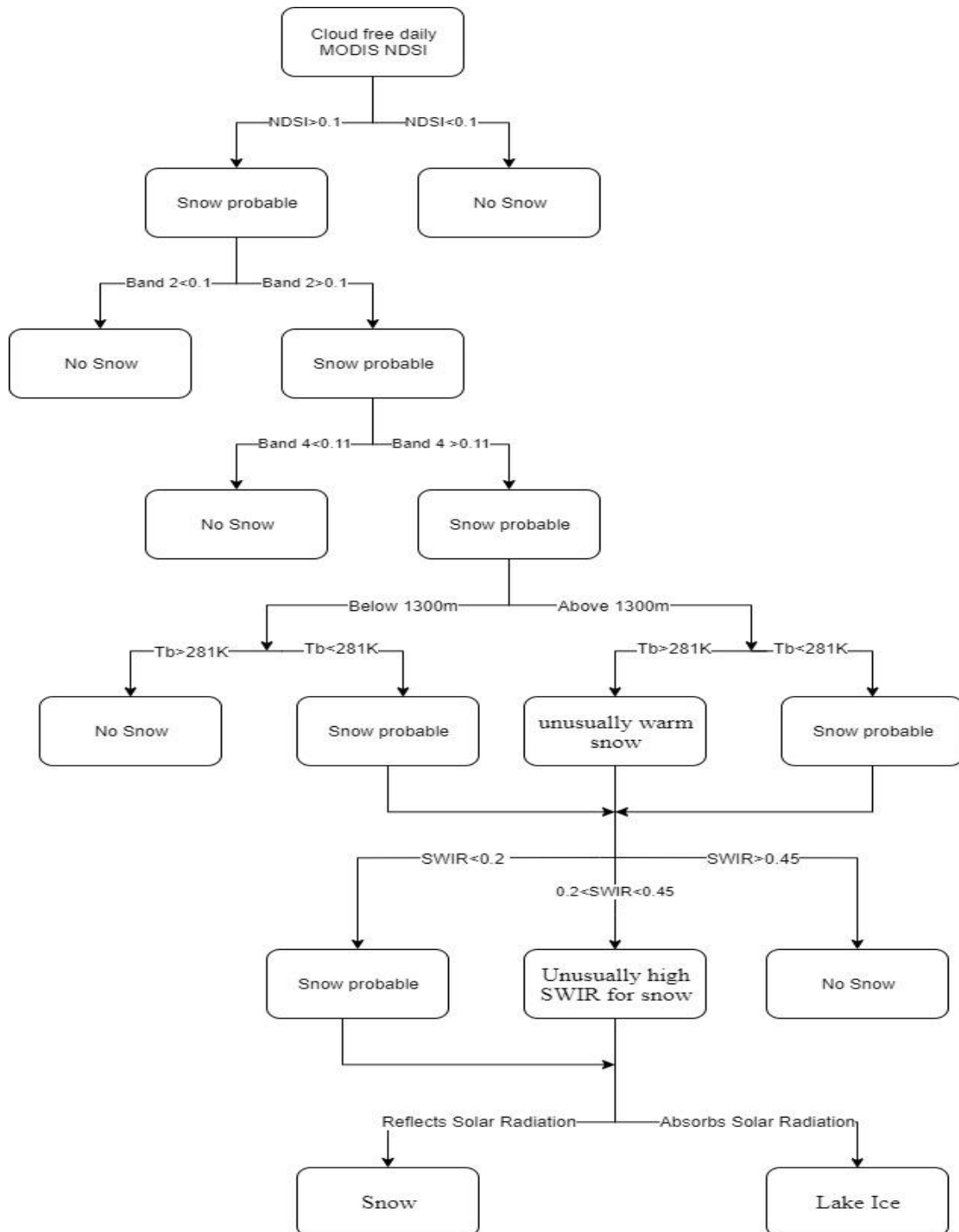


Figure 3. Flow chart of the MODIS Snow detection algorithm also used for Landsat

C. Snow cover from Landsat

For the purpose of this study, Landsat 4-5-7-8 surface reflectance was used. Landsat 7 images after 31 May 2003 suffered data loss due to a failure on the scan line corrector of the sensor, which leads to a loss of about 22% per scene. These scenes were gap-filled using the “focal” function from the raster package in R (Hijmans & van Etten, 2014). This function estimates the values of the neighborhood of focal cells (3x3 moving average). Rather than filling the final NDSI product, we filled the bands required for snow area detection, which in this case are the green and near-infrared bands for NDSI calculation.

All of the Landsat images that are available between August 1984 and August 2019 were used and were classified into three categories: firstly the cloud-free images were immediately used, secondly the cloudy images, where the snow cover was not affected by cloud which could underestimate snow extent, and finally, the images that could not be used.

The first step of the Landsat snow area retrieval consisted of cloud removal, this step comprised of using the Landsat Pixel_qa band, namely bit 3: Cloud Shadow, and bit 5: Cloud. Once the clouds were removed, NSDI could be calculated. Snow cover detection was based on the normalized difference snow index NDSI. This band formula takes advantage of the snow surface reflectance in the green and shortwave infrared

bands, for Landsat 4, 5 and 7 bands two and five were used $NDSI_{L4-5-7} = \frac{Band2 - Band5}{Band2 + Band5}$

For Landsat 8 bands three and six were used $NDSI_{L8} = \frac{Band3 - Band6}{Band3 + Band6}$

Removing snow that was wrongly classified was done using band thresholds, where the pixel that was classified as snow but had an NDSI value lower than 0.4 were

set as no snow. The pixels that had unusual high brightness temperature, higher than 281K, were set to no snow, and all the pixels that had ρ_{SWIR} lower than 0.12 or ρ_{SWIR} higher than 0.16 were classified as no-snow. After going through the screening process, each image was looked at individually to find out whether the snow area was well represented and could be used. Each pixel was changed to a binary product; the area was calculated using the pixel area for each pixel as this function in the Google Earth Engine takes into consideration the curvature of the image, summed for the whole image and plotted in a time series. The next step was producing a daily snow extent time series where the Landsat collection was divided into two groups. The first group extended from February 2000 till August 2019, where the daily MODIS snow extent time series previously calculated could be used.

A seasonal correlation equation was generated between the daily MODIS data and the 8-day Landsat data on each watershed separately. From this equation, the missing Landsat data were filled. For the data before February 2000 where no MODIS data is available, daily precipitation was used to determine the peak snow extent of each snowfall event, by correlating the amount of rainfall to the snow area. Once the peak day was determined, the lowest snow line for each watershed would be visually determined, and the elevation of that snowline would be retrieved. Using the SRTM 30-meter image, the snow area could be determined by assuming that the area above the snow was fully covered. The snow area data was then cubically interpolated between the peak snow day and the closest clear day.

D. Albedo retrieval

Both MODIS MOD10A1 and MYD10A1 have an Albedo band that was used. Albedo was calculated using Landsat 8,7,5,4 surface reflectance using weighting function (Tasumi, Allen, & Trezza, 2008) $\alpha = \sum_{b=1}^n [\rho_{s,b} w_b]$. The weighing coefficients used are band and satellite specific where Landsat 4,5,7 share the same coefficients suggested by Tasumi et al., (2008), and Landsat 8 coefficients used were suggested by Olmedo, (2017) (Table 3). The retrieved Landsat and MODIS albedo were correlated with surface density retrieved by Fayad et al., (2017) during the 2015 and 2016 snow seasons along the western slopes of Mount Lebanon in three watersheds: Abou Ali, Ibrahim, Kelb.

Table 3. Weighing coefficients for Landsat 4,5,7,8 albedo calculation

	<i>Blue band</i>	<i>Green band</i>	<i>Red band</i>	<i>Near-infrared band</i>	<i>Shortwave-infrared band 1</i>	<i>Shortwave-infrared band 2</i>
<i>Landsat 4-5-7 (Tasumi et al., 2008)</i>	0.254	0.149	0.147	0.311	0.103	0.036
<i>Landsat 8 (Olmedo et al., 2017)</i>	0.246	0.146	0.191	0.304	0.105	0.008

E. Snow Depth retrieval from Sentinel-1

Snow depth retrieval consisted of using the methods explained in (Lievens et al., 2019), which relied on processing Sentinel 1 observations for 2015, 2016 winter seasons, over the western slopes of Mount Lebanon, notably Abou Ali, Ibrahim, Kalb watersheds as AWS depth measurements are available (Fayad, Gascoin, Faour, Fanise, et al., 2017). Google Earth Engine was used for the Sentinel-1 depth analysis as all the

scenes available are pre-processed for thermal noise removal, radiometric calibration, terrain correction with the Sentinel-1 Toolbox. Images were classified based on the incident angle between the ascending and descending. Outliers were removed by rejecting values that are 3 dB above and below the 90th-percentile and 10th-percentile respectively.

The snow depth in meters consisted of an empirical change detection method applied to the cross-polarization ratio ($\sigma_{vh}^0/\sigma_{vv}^0$; in dB) of the cross-polarization (VH) and the co-polarization (VV). We validated snow detection using Landsat and MODIS daily measurements to determine the snow cover days, and the depth of each snowy day was retrieved from the AWS snow depth acoustic sensors and validated by comparing the Sentinel-1 data to the AWS data. A change detection index was used to detect the change at location i and time step t . This index links the temporal changes between Sentinel images with snow accumulation or ablation.

$$SI(i, t) = \begin{cases} \max(0, [SI(i, t-1) + \sigma_{vh}^0/\sigma_{vv}^0(i, t) - \sigma_{vh}^0/\sigma_{vv}^0(i, t-1)]) & \text{if } SC(i, t) = 1 \\ 0 & \text{if } SC(i, t) = 0 \end{cases} \text{ (Lievens et al., 2019)}$$

SI was then rescaled into snow depth in meters using the following equation:

$$SD(i, t) = \left(\frac{a}{1 - bFC(i)} SI(i, t) \right) \text{ (Lievens et al., 2019)}$$

Where a (in m dB-1) and b (dimensionless) are constants in time and space, and FC (dimensionless) is the evergreen forest cover fraction as forests typically attenuate the snow backscatter, either the incoming radiation from reaching the snow or the reflected snow radiation from reaching the satellite. Further smoothing was performed on the time series to reduce observation noise.

F. Correlation of snow area with streamflow

The relationship between snow areas retrieved from Landsat was compared to streamflow in Mm^3 and precipitation (mm) using regression and correlation methods and analyzing the coefficients of determination. The study was done on a seasonal and annual time base on the Litany basin between 1984 and 2011.

G. Correlation of snow area with temperature and precipitation

Correlation between snow area and Temperature consisted of using the mean air temperature in Kelvin at 2 meters height from the ERA5 Daily aggregates - Latest climate reanalysis produced by ECMWF / Copernicus Climate Change Service between 1984 and 2019. Once the dataset was chosen and restricted to the date and clipped to the study area, which in this case we restricted the analysis over the main four basins: North, South, East, West, the daily temperature could be retrieved. The daily temperature data was aggregated into seasonal values by averaging the temperature during those months. The seasonal analysis consisted of splitting each year into four seasons named DJF denoting December, January, February as the winter season, MAM denoting March, April, May as the spring season, JJA denoting June, July, August as the summer season, and SON denoting September, October, November as the Fall season. The same seasonal analysis was applied to different parts of this research. Lastly, statistical analysis was done on the temperature time series, and a correlation analysis was done between seasonal snow area and seasonal temperature.

For the precipitation analysis, the precipitation band in mm/day from the CHIRPS Daily: Climate Hazards Group InfraRed Precipitation with Station Data

(version 2.0 final) was used. The methodology for time series analysis of precipitation and correlation with snow area data is similar to the seasonal temperature analysis, with the only difference being the addition of the daily precipitation values to produce the seasonal precipitation data rather than averaging the values.

H. Trend Analysis and Significance

Trend analysis was tested using the eWater toolkit TREND program that tests time series data for trend significance, change, and randomness (Grayson, 1996; Kundzewicz & Robson, 2000). All 12 of the statistical tests provided were applied to all the time-series analyses in this research. Statistical tests include Mann-Kendall to test whether there is a trend in the time series data; the rest of the tests can be found in table 4. TREND will display the value of the test named test statistics, as an example, the z-statistics for the Man-Kendall test, the critical values of the test at significance levels of $\alpha = 0.01$, $\alpha = 0.05$ and $\alpha = 0.1$, a statement of the test result, critical values of the test obtained from the resampling analysis (Grayson, 1996; Kundzewicz & Robson, 2000).

Table 4. Trend analysis and Significance Tests

<i>Test name</i>	<i>Statistical test</i>
<i>Spearman's Rho</i>	Rank-based test that determines whether the correlation between two variables is significant
<i>Linear Regression</i>	Tests whether there is a linear trend by examining the relationship between time (x) and the variable of interest (y).,
<i>Distribution-free CUSUM</i>	Tests whether the means in two parts of a record are different
<i>Cumulative Deviation</i>	Tests whether the means in two parts of a record are different
<i>Worsley Likelihood</i>	Tests whether the means in two parts of a record are different
<i>Rank-Sum</i>	Tests whether the medians in two different periods are different
<i>Student's t</i>	Tests whether the means in two different periods are different
<i>Median Crossing</i>	Tests whether the medians in two different periods are different
<i>Turning Points</i>	Test of the independence of a series of random variables
<i>Rank Difference</i>	Tests, whether the rank means in two different periods, are different
<i>Autocorrelation</i>	The degree of similarity between the values over successive time intervals

CHAPTER IV

RESULTS AND DISCUSSION

In this section, we limited the data analysis to 4 areas, dividing the full research region into North, South, East, and West. Only three of the four seasons were analyzed, discarding the summer season (JJA) between June and August as it had no significance. Using the previously stated datasets, the snow cover days, snow cover area, and Albedo were extracted from Landsat, MODIS, while snow depth from Sentinel1 and streamflow was correlated with snow, are from Landsat. Results for other sub-areas are in the Appendix.

A. Landsat, MODIS snow detection and snow cover days

As MODIS data began during February 2000, the comparison between MODIS and Landsat snow detection was restricted to the overlap period of 2000 and 2019. Seeing as the same methodology was used on both datasets, the difference in snow detection sensitivity between the two products is attributed to the pixel size.

Pixel size is not a significant concern in large study areas with relatively flat terrain, but seeing as the study area is a mountainous region, the pixel size will have a significant effect on snow detection. The major difference in snow detection between MODIS and Landsat can be observed during mid-season where the MODIS analysis will overestimate the snow cover area (Figure 4) while underestimate the snow area during late season at the border of the snow area, between snowy and non-snowy pixels and especially with ephemeral snow, where smaller and smaller snow patches can be

picked up using the Landsat analysis but considered as non-snow pixels with MODIS, for example, figure 5 taken on the 5th of July 2019, where the Landsat image (Left) has easily picked up the last season snow and the MODIS image (Right) failed to pick it up.

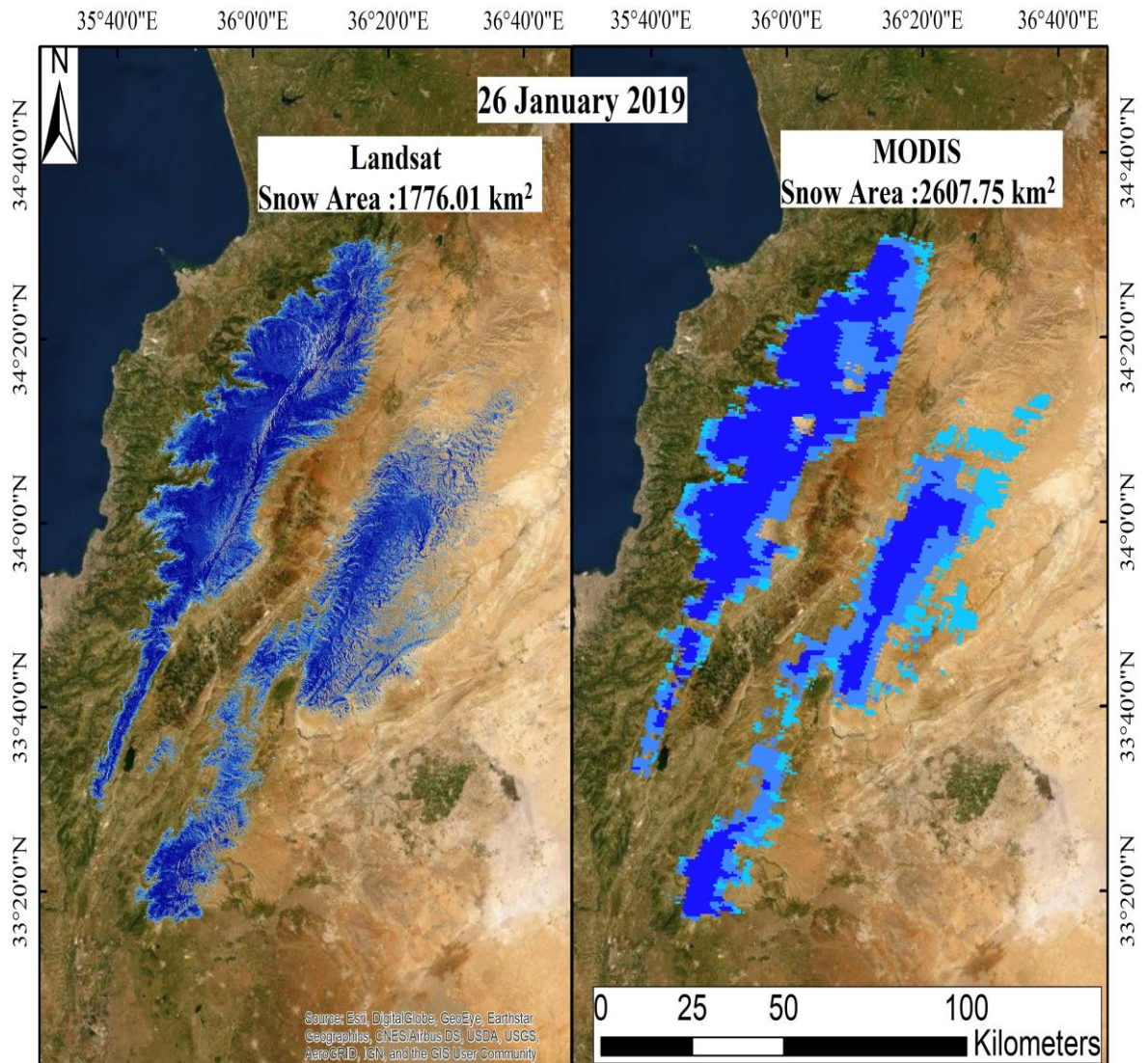


Figure 4. Comparison between Mid-Season Landsat (left) and MODIS (right) snow detection

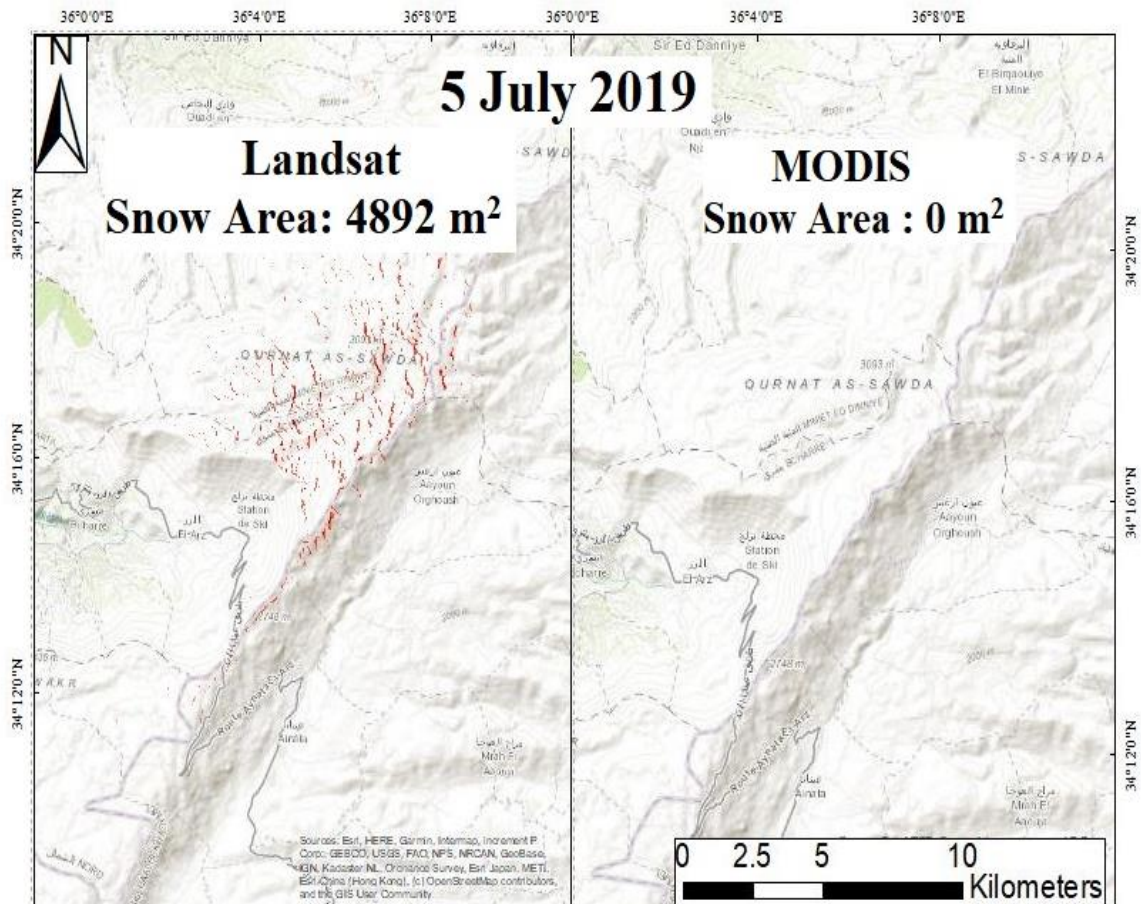


Figure 5. Comparison between Late-Season Landsat (left) and MODIS (right) snow detection

Another parameter affected by the large MODIS pixel size compared to Landsat is the Snow Cover Days. Snow cover days take into consideration the number of days with snow cover in an area. Snow cover days were calculated on an annual basis where the snow detection algorithm for NDSI and Landsat could pick up snow cover. Figure 6 shows the snow detection comparison between Landsat and MODIS shows clearly the higher detection sensitivity of Landsat.

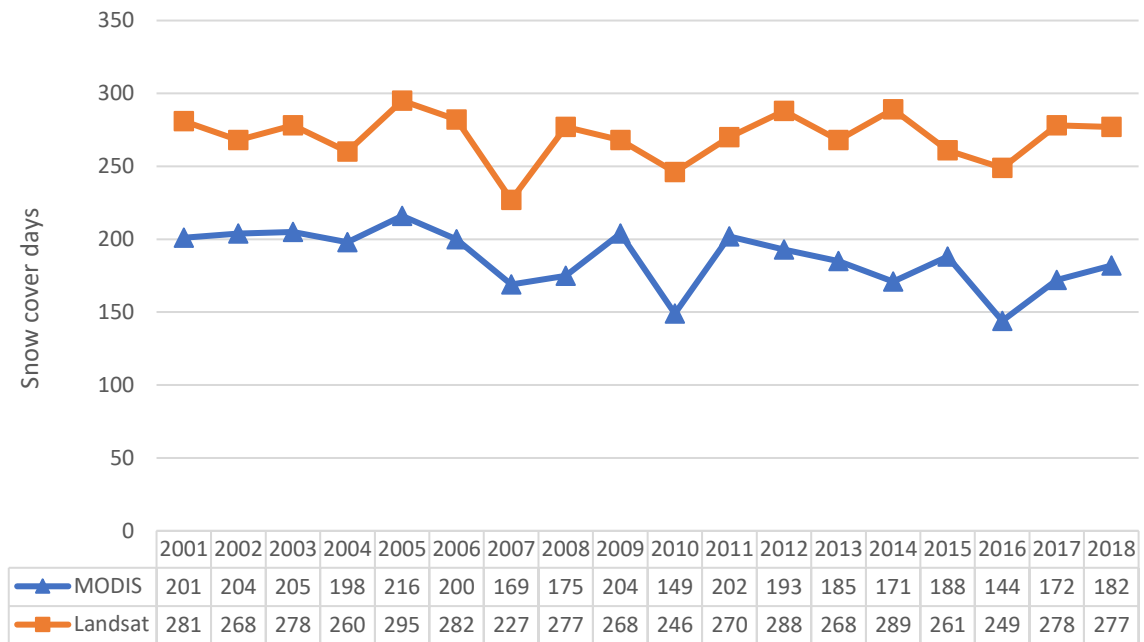


Figure 6. Landsat and MODIS annual Snow Cover days between 2001 and 2018

B. Snow days Trend

For the snow cover days analysis, the results were extracted and analyzed during the summer of 2019. Over the whole study area, both Landsat and MODIS snow cover days trend analysis showed a decreasing trend. MODIS showed a decreasing trend of about 2.1 days/year as it was restricted between 2001 and 2018 (Figure 7). Landsat showed a non-significant decreasing trend of about 0.08 days/year between 1985 and 2018 (Figure 8). Landsat snow cover days did not show any significance when analyzed over the whole area. MODIS snow cover days analysis showed significance with a 2006-year mean change when analyzed over the whole area (Table 5).

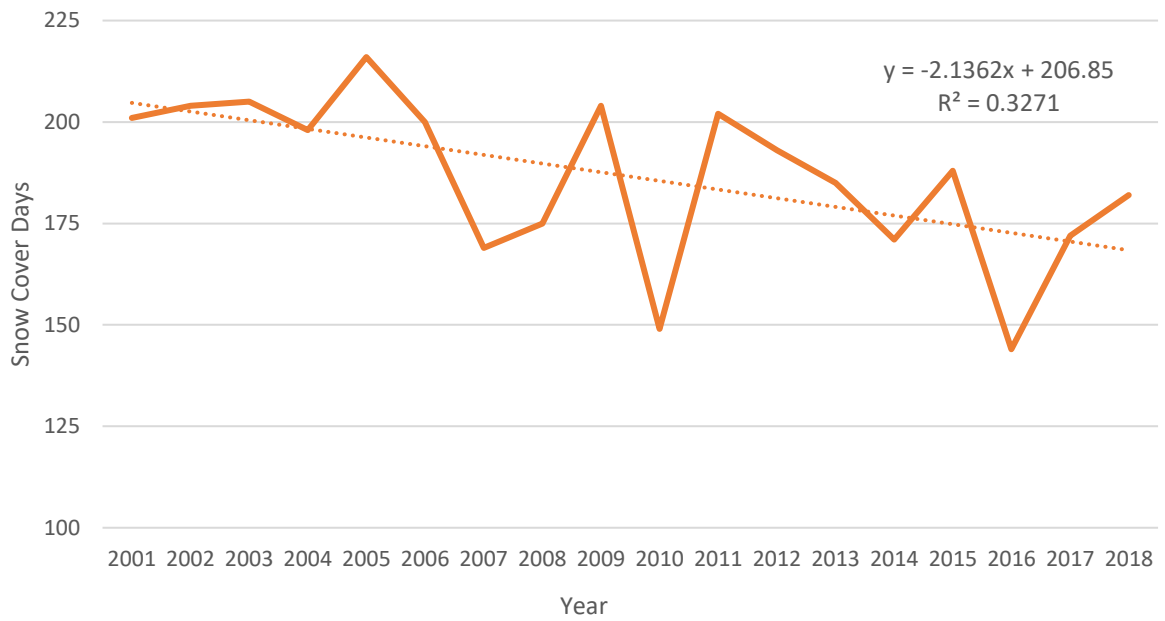


Figure 7. Annual MODIS Snow Cover Days for the whole study area

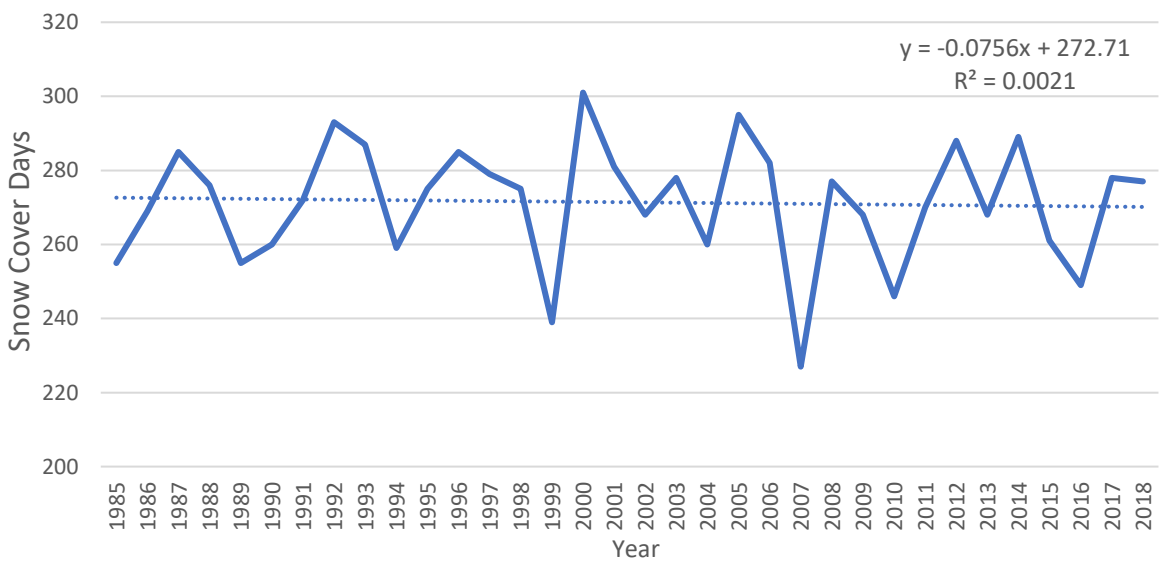


Figure 8. Annual Landsat Snow Cover Days for the whole area

Between 2000 and 2018, a negative trend for snow cover days dominated all basins retrieved with the MODIS dataset, showing the highest value in the northern and

western basins with a decrease of around two days/year. For the southern and eastern basins, the negative slope was about 1.7 days/year (Figure 9). The MODIS snow cover day's analyses showed significance over all the watersheds using different methods; most importantly, with the Man-Kendall test showing good significance at 0.01 for the western and northern watersheds, a 0.05 and 0.1 significance for the south and eastern watersheds respectively (Table 5).

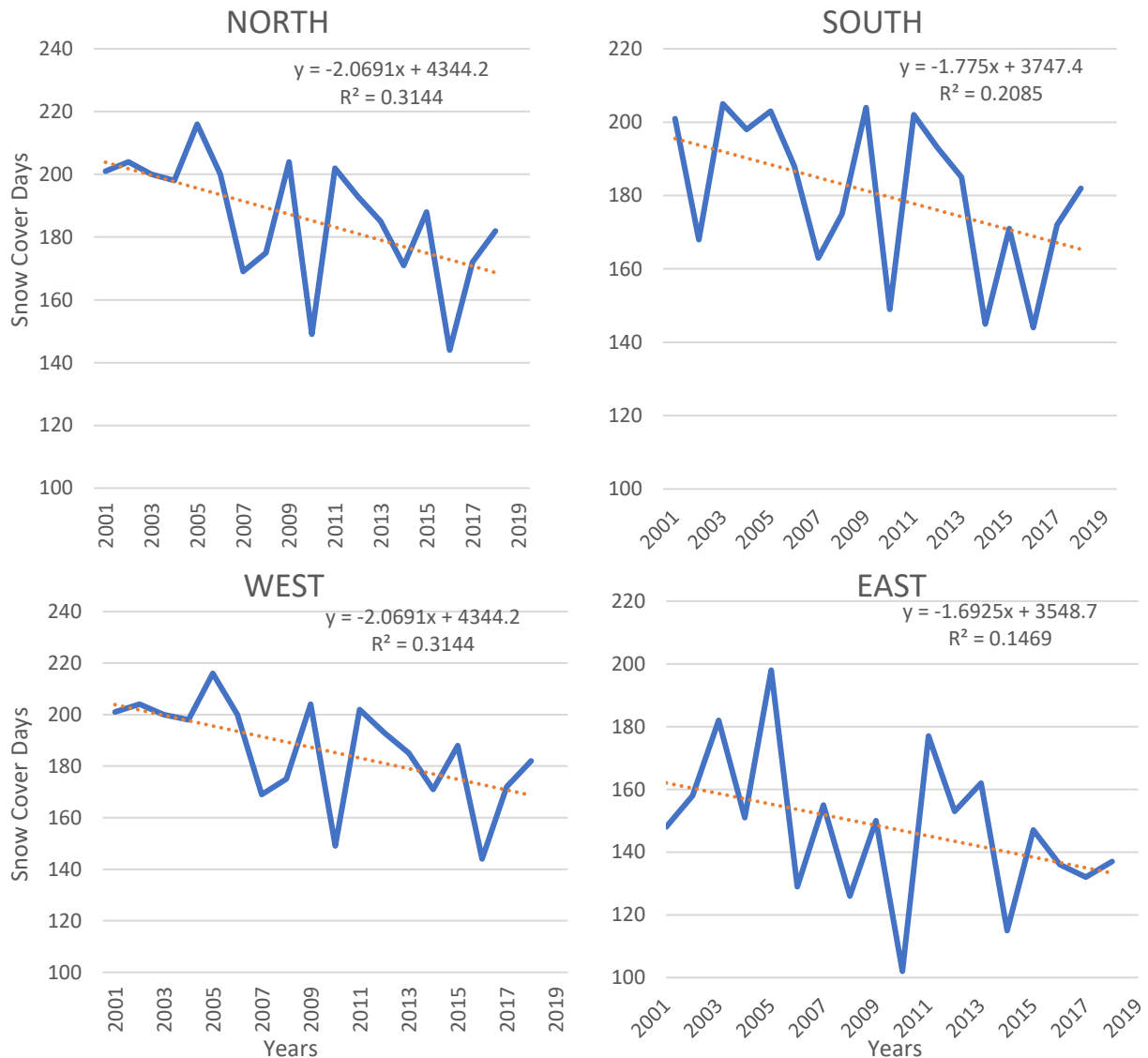


Figure 9. MODIS annual snow cover days over the north, south, east, and west basins

Table 5. MODIS trend results for the annual snow cover days over the north, east, west, and south basins

Year of change	Basin	Statistical test	Test statistic	Critical Value at 0.1	Critical Value at 0.05	Critical Value at 0.01	Result
2006	Lebanon	Mann-Kendall	-2.462	1.398	1.666	2.19	<i>S (0.01)</i>
2006	Lebanon	Spearman's Rho	-2.515	1.398	1.666	2.19	<i>S (0.01)</i>
2006	Lebanon	Linear regression	-2.789	1.746	2.12	2.921	<i>S (0.05)</i>
2006	Lebanon	Cusum	6	5.176	5.77	6.916	<i>S (0.05)</i>
2006	Lebanon	Cumulative deviation	1.273	1.09	1.204	1.394	<i>S (0.05)</i>
2006	Lebanon	Worsley likelihood	3.302	2.928	3.312	4.206	<i>S (0.1)</i>
2006	Lebanon	Rank Sum	2.563	1.398	1.666	2.19	<i>S (0.01)</i>
2006	Lebanon	Student's t	2.4	1.74	2.11	2.898	<i>S (0.05)</i>
2006	Lebanon	Median Crossing	1.698	1.398	1.666	2.19	<i>S (0.05)</i>
2005	East	Mann-Kendall	-1.515	1.398	1.666	2.19	<i>S (0.1)</i>
2005	East	Spearman's Rho	-1.647	1.398	1.666	2.19	<i>S (0.1)</i>
2005	East	Turning Point	1.965	1.398	1.666	2.19	<i>S (0.05)</i>
2006	North	Mann-Kendall	-2.424	1.398	1.666	2.19	<i>S (0.01)</i>
2006	North	Spearman's Rho	-2.396	1.398	1.666	2.19	<i>S (0.01)</i>
2006	North	Linear regression	-2.709	1.746	2.12	2.921	<i>S (0.05)</i>
2006	North	Cusum	6	5.176	5.77	6.916	<i>S (0.05)</i>
2006	North	Cumulative deviation	1.248	1.09	1.204	1.394	<i>S (0.05)</i>
2006	North	Worsley likelihood	3.192	2.928	3.312	4.206	<i>S (0.1)</i>
2006	North	Rank Sum	2.267	1.398	1.666	2.19	<i>S (0.01)</i>
2006	North	Student's t	2.305	1.74	2.11	2.898	<i>S (0.05)</i>
2006	North	Median Crossing	1.698	1.398	1.666	2.19	<i>S (0.05)</i>
2013	South	Mann-Kendall	-1.97	1.398	1.666	2.19	<i>S (0.05)</i>
2013	South	Spearman's Rho	-1.868	1.398	1.666	2.19	<i>S (0.05)</i>
2013	South	Linear regression	-2.053	1.746	2.12	2.921	<i>S (0.1)</i>
2013	South	Rank Sum	-2.107	1.398	1.666	2.19	<i>S (0.05)</i>
2013	South	Student's t	1.992	1.74	2.11	2.898	<i>S (0.1)</i>
2006	West	Mann-Kendall	-2.424	1.398	1.666	2.19	<i>S (0.01)</i>
2006	West	Spearman's Rho	-2.396	1.398	1.666	2.19	<i>S (0.01)</i>
2006	West	Linear regression	-2.709	1.746	2.12	2.921	<i>S (0.05)</i>
2006	West	Cusum	6	5.176	5.77	6.916	<i>S (0.05)</i>
2006	West	Cumulative deviation	1.248	1.09	1.204	1.394	<i>S (0.05)</i>
2006	West	Worsley likelihood	3.192	2.928	3.312	4.206	<i>S (0.1)</i>
2006	West	Rank Sum	2.267	1.398	1.666	2.19	<i>S (0.01)</i>
2006	West	Student's t	2.305	1.74	2.11	2.898	<i>S (0.05)</i>
2006	West	Median Crossing	1.698	1.398	1.666	2.19	<i>S (0.05)</i>

Between 1985 and 2018, a negative trend for snow cover days dominated all

basins retrieved with the Landsat datasets, showing the highest value in the eastern

basin with a decrease of around one day/year. For the northern basin, the negative slope is about 0.05 days/year. For the southern basin, the negative slope is about 0.54 days/year. For the Western basin, the negative slope is about 0.07 days/year (Figure 10). The Landsat snow cover days showed significance with different test but mainly showing significance using the Man-Kendall test in the eastern watershed at 0.1 significance level (Table 6).

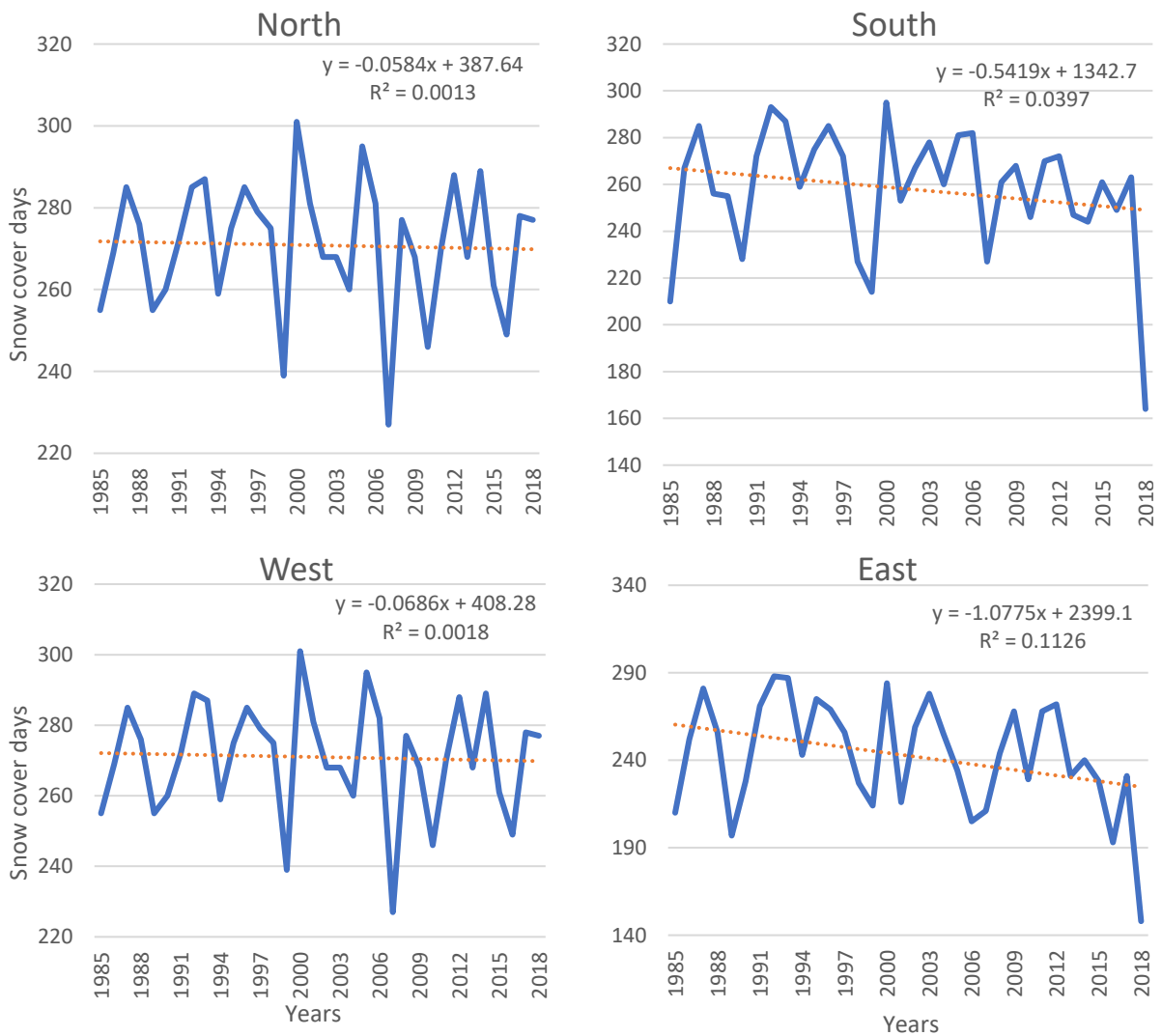


Figure 10. Landsat annual snow cover days over the north, south, east, and west basins

Table 6. Landsat trend results for the annual snow cover days over the whole area, north, east, west, and south basins

Year of change	Basin	Statistical test	Test statistic	Critical Value at 0.1	Critical Value at 0.05	Critical Value at 0.01	Result
2004	East	Mann-Kendall	-1.749	1.645	1.96	2.576	<i>S (0.1)</i>
2004	East	Linear regression	-2.015	1.694	2.038	2.741	<i>S (0.1)</i>
2004	East	Worsley likelihood	3.468	2.876	3.206	3.868	<i>S (0.05)</i>
2004	East	Rank Sum	-1.873	1.645	1.96	2.576	<i>S (0.1)</i>
2004	East	Student's t	1.963	1.693	2.036	2.736	<i>S (0.1)</i>
2004	East	Turning Point	-1.812	1.645	1.96	2.576	<i>S (0.1)</i>
2006	North	Turning Point	-1.812	1.645	1.96	2.576	<i>S (0.1)</i>
2006	South	Worsley likelihood	4.394	2.876	3.206	3.868	<i>S (0.01)</i>
2006	West	Turning Point	-1.812	1.645	1.96	2.576	<i>S (0.1)</i>

C. Landsat Snow Cover Area

Based on the above methodology for SCA retrieval from Landsat, 47 Landsat 4 scenes, 916 Landsat 5 scenes, 669 Landsat 7 scenes, and 278 Landsat 8 scenes were used. The results for the mean annual area showed that between the snow seasons of 1984-1985 and 2018-2019, taking into consideration that the basins have overlapping areas (Figure 2). The annual average snow area in km² peaked during the 1991-1992 winter season for all four areas and showed the lowest average area during the 2009-2010 (Figure 11) with a decreasing trend overall basins, which will be discussed later.

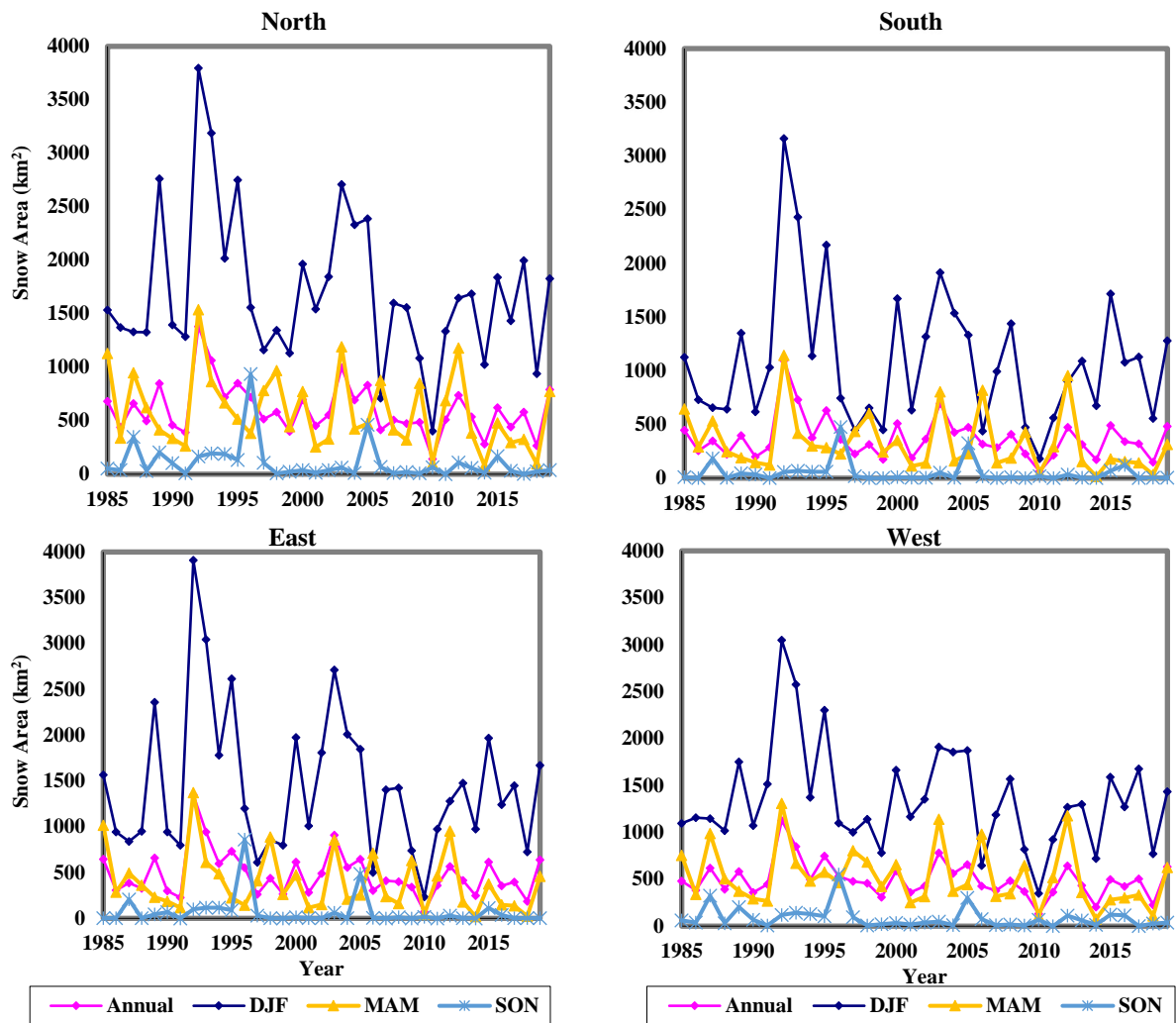


Figure 11. Annual and Seasonal average Snow Area km^2 over the north, south, east, and west areas

D. Landsat Trend Analysis

We present the results for the north, south, east, and west basins trend analysis for the snow area retrieved between 1984 and 2019 from Landsat 4-5-7-8. For the north, south, east, and west basins, the trend is negative, ranging between a decrease of 9 km^2/year for the northern basin, 5.1 km^2/year for the Southern, and around 7.4 km^2/year for both eastern and western basins (Figure12). No significance was observed with the south watershed trend analysis. The North, West, East watersheds 5-year moving average trend analysis showed significance, where the eastern watershed only showed

significance with the Student-t test, while the North, and South showed good significance with five and four statistics tests respectively apart from the Mann-Kendall test, with a 2005-year mean change for all watersheds (Table 8). With the removal of the 1992 peak snow season, we still noticed a significant decreasing trend in the northern and western basins (Figure 13).

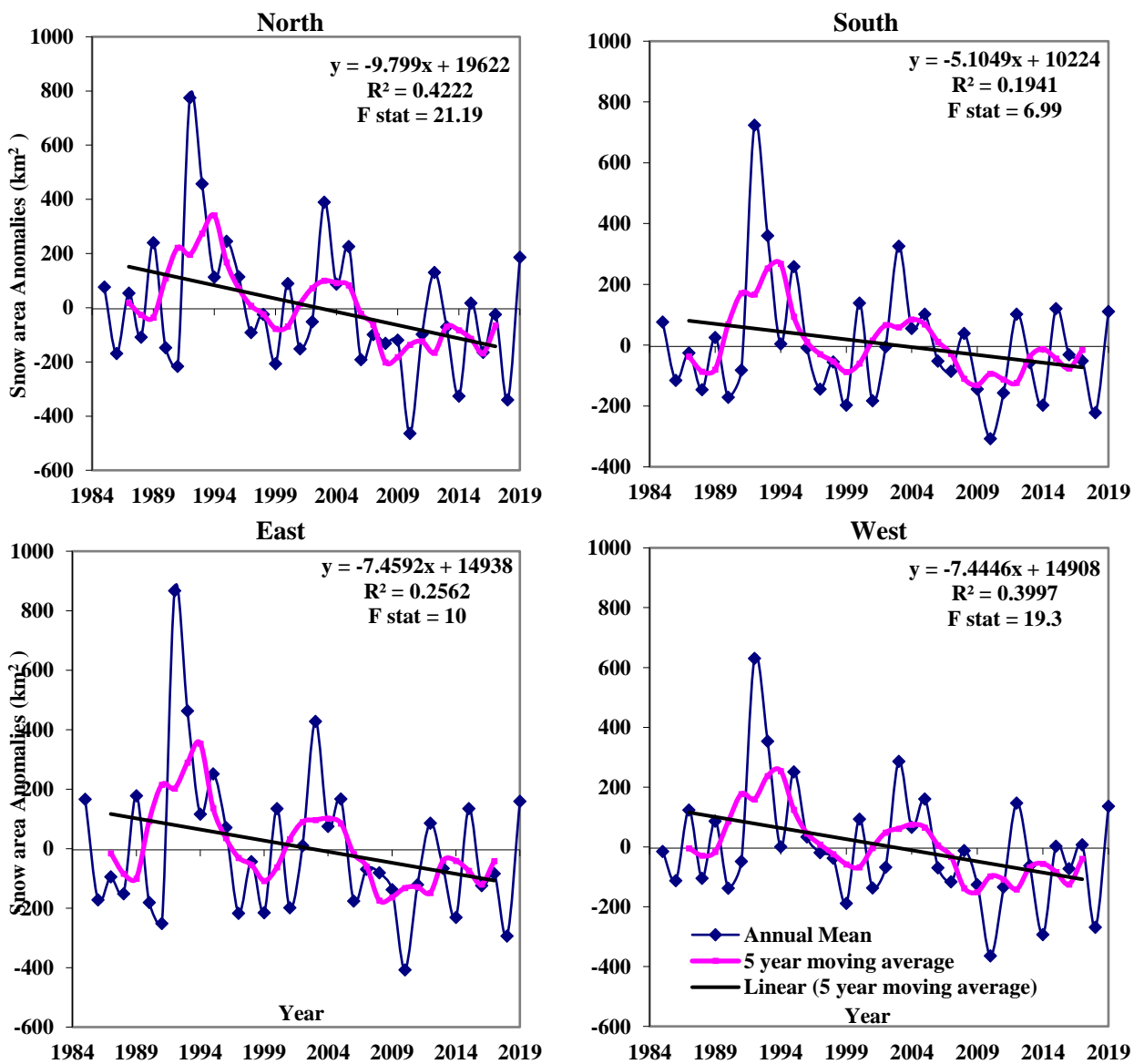


Figure 12. Annual average Snow Area Anomalies km² over the north, south, east, and west areas

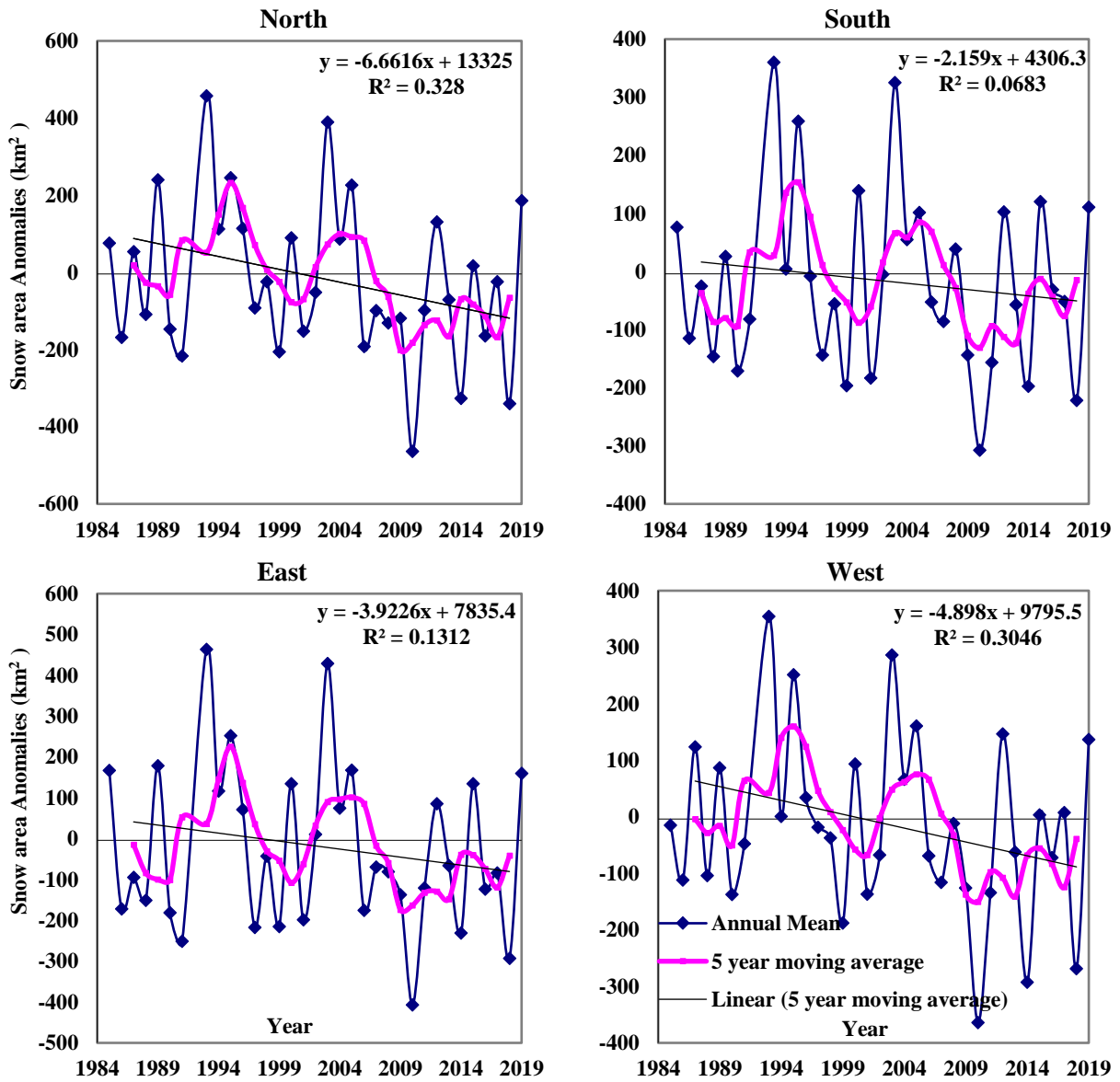


Figure 13. Annual average Snow Area Anomalies km^2 over the north, south, east, and west areas without the 1992 snow season.

Table 7. Landsat annual trend results for the snow cover area anomalies over the north, east, west, and south basins.

Year of change	Basin	Statistical test	Test statistic	Critical Value at 0.1	Critical Value at 0.05	Critical Value at 0.01	Result
2005	EAST	Student's t	1.758	1.692	2.034	2.732	<i>S</i> (0.1)
2005	NORTH	Linear regression	-1.883	1.693	2.036	2.736	<i>S</i> (0.1)
2005	NORTH	Cumulative deviation	1.234	1.125	1.25	1.48	<i>S</i> (0.1)
2005	NORTH	Rank Sum	-1.85	1.645	1.96	2.576	<i>S</i> (0.1)
2005	NORTH	Student's t	2.146	1.692	2.034	2.732	<i>S</i> (0.05)
2005	NORTH	Turning Point	2.058	1.645	1.96	2.576	<i>S</i> (0.05)
2005	WEST	Linear regression	-1.756	1.693	2.036	2.736	<i>S</i> (0.1)
2005	WEST	Cumulative deviation	1.129	1.125	1.25	1.48	<i>S</i> (0.1)
2005	WEST	Rank Sum	-1.65	1.645	1.96	2.576	<i>S</i> (0.1)
2005	WEST	Student's t	1.968	1.692	2.034	2.732	<i>S</i> (0.1)

The trend analysis also involves a seasonal analysis, where the annual snow was also analyzed on a seasonal basis. The trend results for the DJF, MAM, SON were analyzed, while JJA was not analyzed as the snow area trend during the summer season is insignificant.

We present the seasonal trend analysis for the four main basins: North, South, and East, West results show that for all basins the snow area peaked during the 1992 snow season and showed the lowest value during the 2010 season. During the winter (DJF) season, a negative trend dominated all basins, showing the highest value in the northern basin with a decrease of around 26 km²/year. For the southern basin, the negative slope was about 14 km²/year. For the Eastern basin, the negative slope was about 21 km²/year. For the Western basin, the negative slope was about 19.2 km²/year (Figure 14). During the winter season, all the watersheds showed significance with a 2005-year mean change apart from the South watershed that had a 1996-year mean change, none of the areas had significance with the Mann-Kendall test (Table 9).

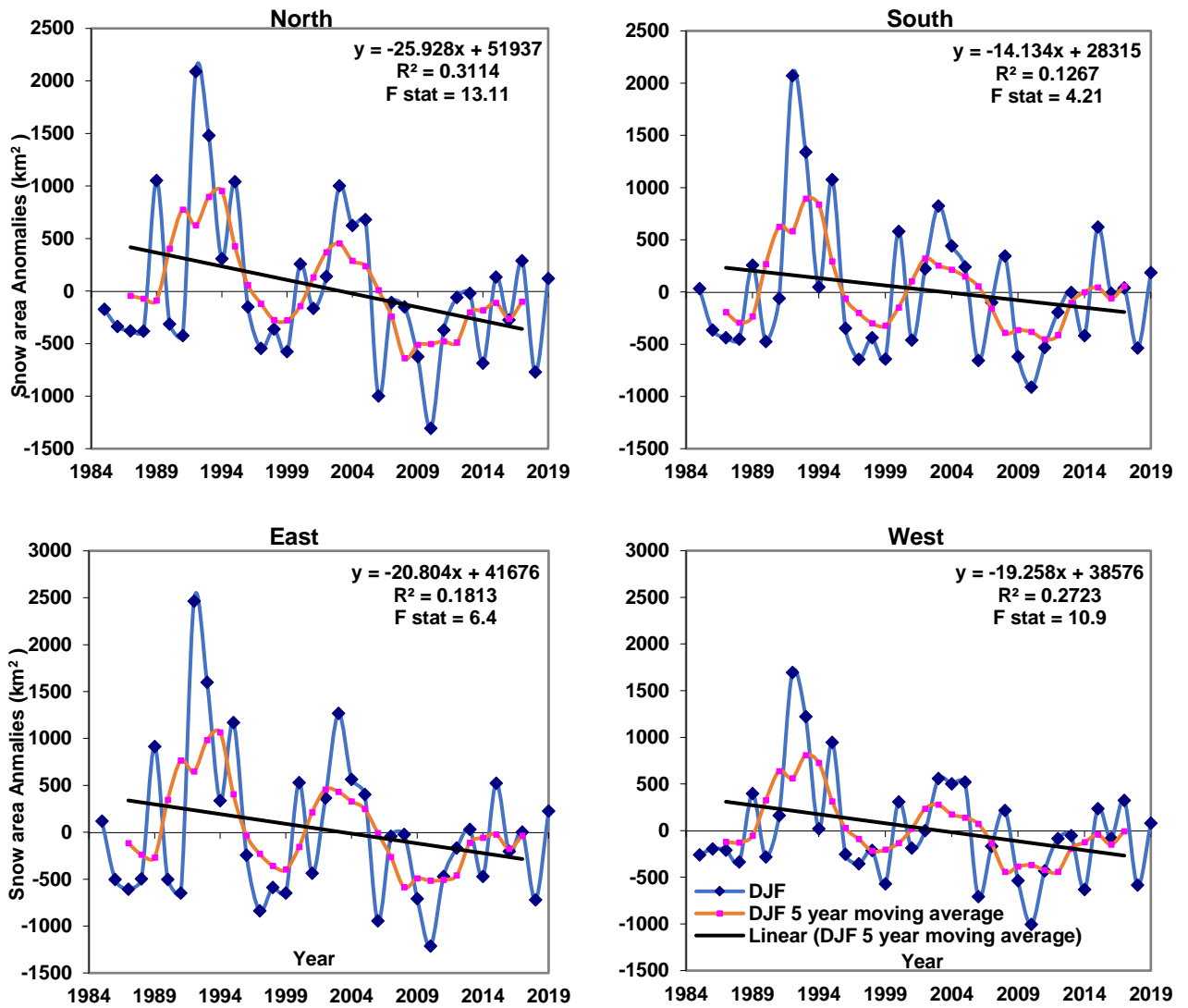


Figure 14. Winter average Snow Area Anomalies km² over the north, south, east, and west areas

During the spring (MAM) season, a negative trend dominated all basins, showing the highest value in the northern basin with a decrease of 8.75 km²/year. For the southern basin, the negative slope was about five km²/year. For the Eastern basin, the negative slope was about 6.2 km²/year. For the Western basin, the negative slope was about 7.6 km²/year (Figure 15). During the spring season, all watersheds showed significance especially with the Mann-Kendall test, where the North, East, West

watersheds showed significance at 0.1, while the southern watershed showed significance at 0.05, with a 2000-year mean change for the Eastern and Western watersheds and a 2012-year mean change for the Southern and Northern watersheds (Table 9).

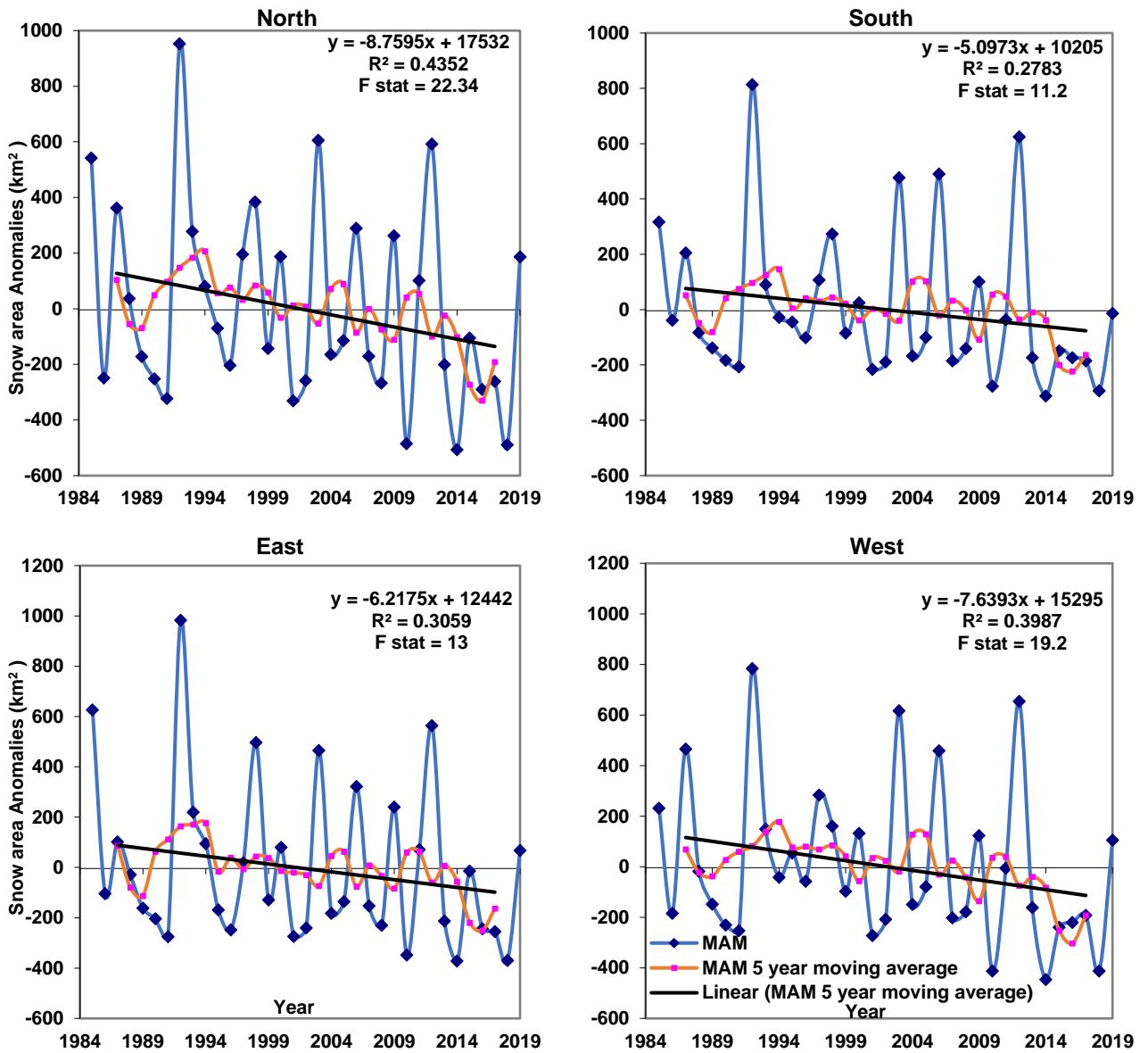


Figure 15. Spring average Snow Area Anomalies km² over the north, south, east, and west areas

During the Fall (SON) season, a negative trend dominated all basins, showing the highest value in the northern basin with a decrease of 5 km²/year. For the southern basin, the negative slope was about 1.5 km²/year. For the Eastern basin, the negative slope was about 3.3 km²/year. For the Western basin, the negative slope was about 3.2 km²/year (Figure 16). For the Fall season, only the North and South watersheds showed significance, most importantly with the Mann-Kendall test at 0.05 for the north with a 1996-year mean change and 0.1 for the West with a 1997-year mean change.

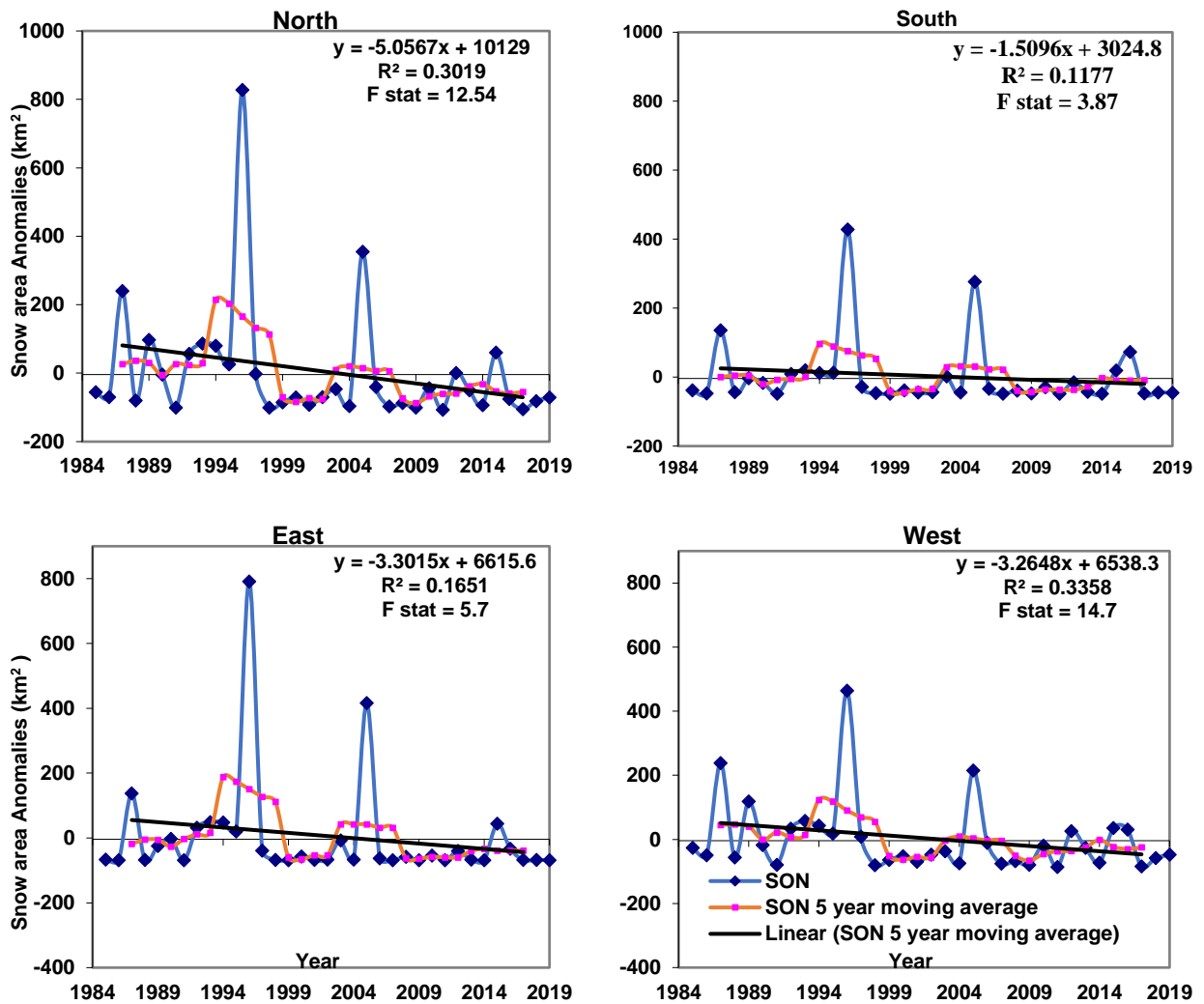


Figure 16. Fall average Snow Area Anomalies km² over the north, south, east, and west areas

Table 8. Landsat seasonal trend results for the snow cover area anomalies over the north, east, west, and south basins.

Year of change	Basin	Season	Statistical test	Test statistic	Critical Value at 0.1	Critical Value at 0.05	Critical Value at 0.01	Result
2005	East	DJF	Student's t	1.845	1.692	2.034	2.732	<i>S (0.1)</i>
2005	East	DJF	Auto Correlation	1.754	1.645	1.96	2.576	<i>S (0.1)</i>
1992	East	JJA	Mann-Kendall	-1.775	1.645	1.96	2.576	<i>S (0.1)</i>
2000	East	MAM	Mann-Kendall	-1.875	1.645	1.96	2.576	<i>S (0.1)</i>
2000	East	MAM	Spearman's Rho	-1.756	1.645	1.96	2.576	<i>S (0.1)</i>
2005	North	DJF	Cumulative deviation	1.181	1.125	1.25	1.48	<i>S (0.1)</i>
2005	North	DJF	Student's t	2.023	1.692	2.034	2.732	<i>S (0.1)</i>
2005	North	DJF	Auto Correlation	1.788	1.645	1.96	2.576	<i>S (0.1)</i>
2012	North	MMA	Mann-Kendall	-1.761	1.645	1.96	2.576	<i>S (0.1)</i>
2012	North	MMA	Spearman's Rho	-1.668	1.645	1.96	2.576	<i>S (0.1)</i>
1996	North	SON	Mann-Kendall	-2.073	1.645	1.96	2.576	<i>S (0.05)</i>
1996	North	SON	Spearman's Rho	-2.094	1.645	1.96	2.576	<i>S (0.05)</i>
1996	North	SON	Rank Sum	2.15	1.645	1.96	2.576	<i>S (0.05)</i>
1996	South	DJF	Auto Correlation	1.818	1.645	1.96	2.576	<i>S (0.1)</i>
1993	South	JJA	Worsley likelihood	3.089	2.88	3.21	3.87	<i>S (0.1)</i>
2012	South	MAM	Mann-Kendall	-1.988	1.645	1.96	2.576	<i>S (0.05)</i>
2012	South	MAM	Spearman's Rho	-1.944	1.645	1.96	2.576	<i>S (0.1)</i>
2012	South	MAM	Rank Sum	-1.67	1.645	1.96	2.576	<i>S (0.1)</i>
2005	West	DJF	Student's t	1.817	1.692	2.034	2.732	<i>S (0.1)</i>
2005	West	DJF	Auto Correlation	1.874	1.645	1.96	2.576	<i>S (0.1)</i>
1993	West	JJA	Worsley likelihood	3.083	2.88	3.21	3.87	<i>S (0.1)</i>
2000	West	MAM	Mann-Kendall	-1.903	1.645	1.96	2.576	<i>S (0.1)</i>
2000	West	MAM	Spearman's Rho	-1.855	1.645	1.96	2.576	<i>S (0.1)</i>
2000	West	MAM	Rank Sum	1.683	1.645	1.96	2.576	<i>S (0.1)</i>
1997	West	SON	Mann-Kendall	-1.676	1.645	1.96	2.576	<i>S (0.1)</i>
1997	West	SON	Spearman's Rho	-1.704	1.645	1.96	2.576	<i>S (0.1)</i>
1997	West	SON	Cumulative deviation	1.15	1.125	1.25	1.48	<i>S (0.1)</i>
1997	West	SON	Rank Sum	2.52	1.645	1.96	2.576	<i>S (0.05)</i>
1997	West	SON	Student's t	2.358	1.692	2.034	2.732	<i>S (0.05)</i>

E. MODIS snow cover area

Based on the above methodology for SCA retrieval from MODIS. All of 7066 out of the 7128 Images for Terra (99.1%) and 6251 out of the 6267 (99.7%) scenes for Aqua were available on GEE were used. The results for the mean annual area showed that between the snow seasons of 2000 and 2019, the annual average snow area in km² peaked during the 2002 winter season for all four areas and showed the lowest average area during the 2014 season (Figure 17).

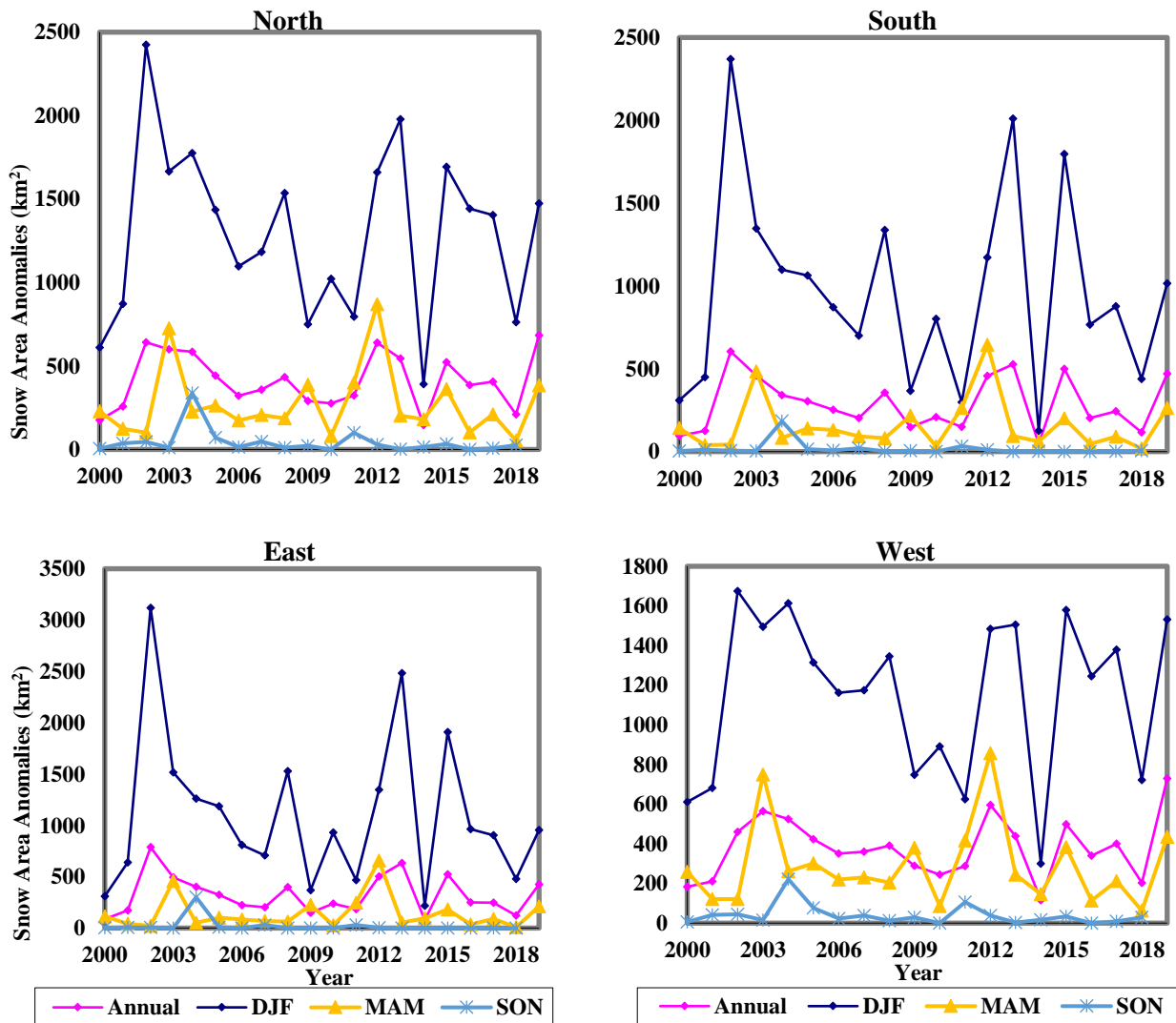


Figure 17. Annual and Seasonal average Snow Area km² over the north, south, east and west areas

F. MODIS Trend Analysis

We present the results for the north, south, east, and west basins trend analysis for the snow area retrieved between 2000 and 2019 from the MODIS MOD10A1 and MYD10A1 daily snow cover product. For the rest of the basins, the results can be found in the Appendix. For the north, south, east, and west basins, the trend is negative, ranging between a decrease of 4.9 km²/year for the northern basin, 3.1 km²/year for the Southern, and around 3.9 km²/year and 4.2 km²/year for the western and eastern basins respectively (Figure 18). No Significance was observed for the annual snow area trend analysis.

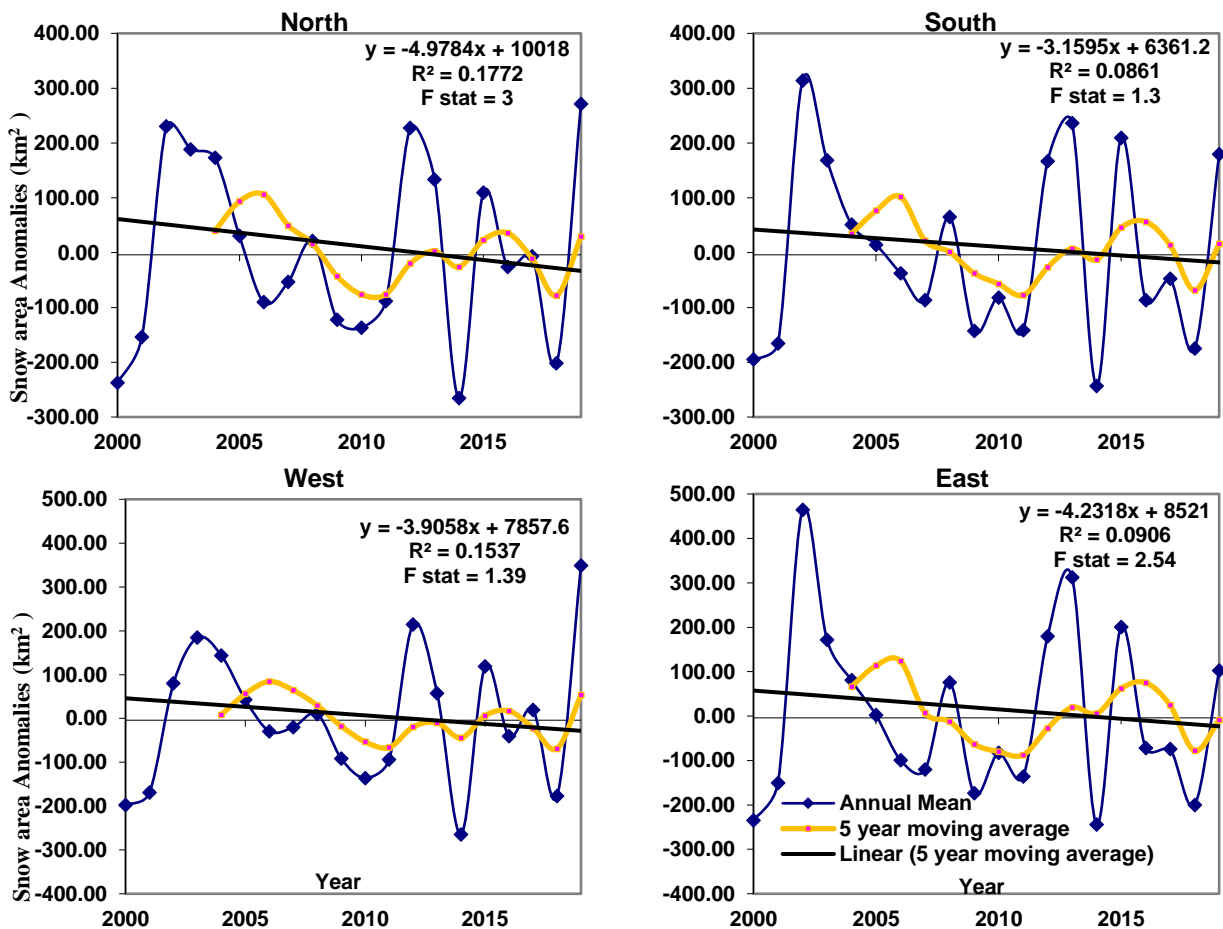


Figure 18. Annual average Snow Area Anomalies km² over the north, south, east, and west areas

During the winter (DJF) season, a negative trend dominated all basins, showing the highest value in the northern basin with a decrease of 17.4 km²/year. For the southern basin, the negative slope was about 12.1 km²/year. For the western basin, the negative slope was about 13.6 km²/year. For the eastern basin, the negative slope was about 16 km²/year (Figure 19). No significance was observed for the winter season snow area trend analysis.

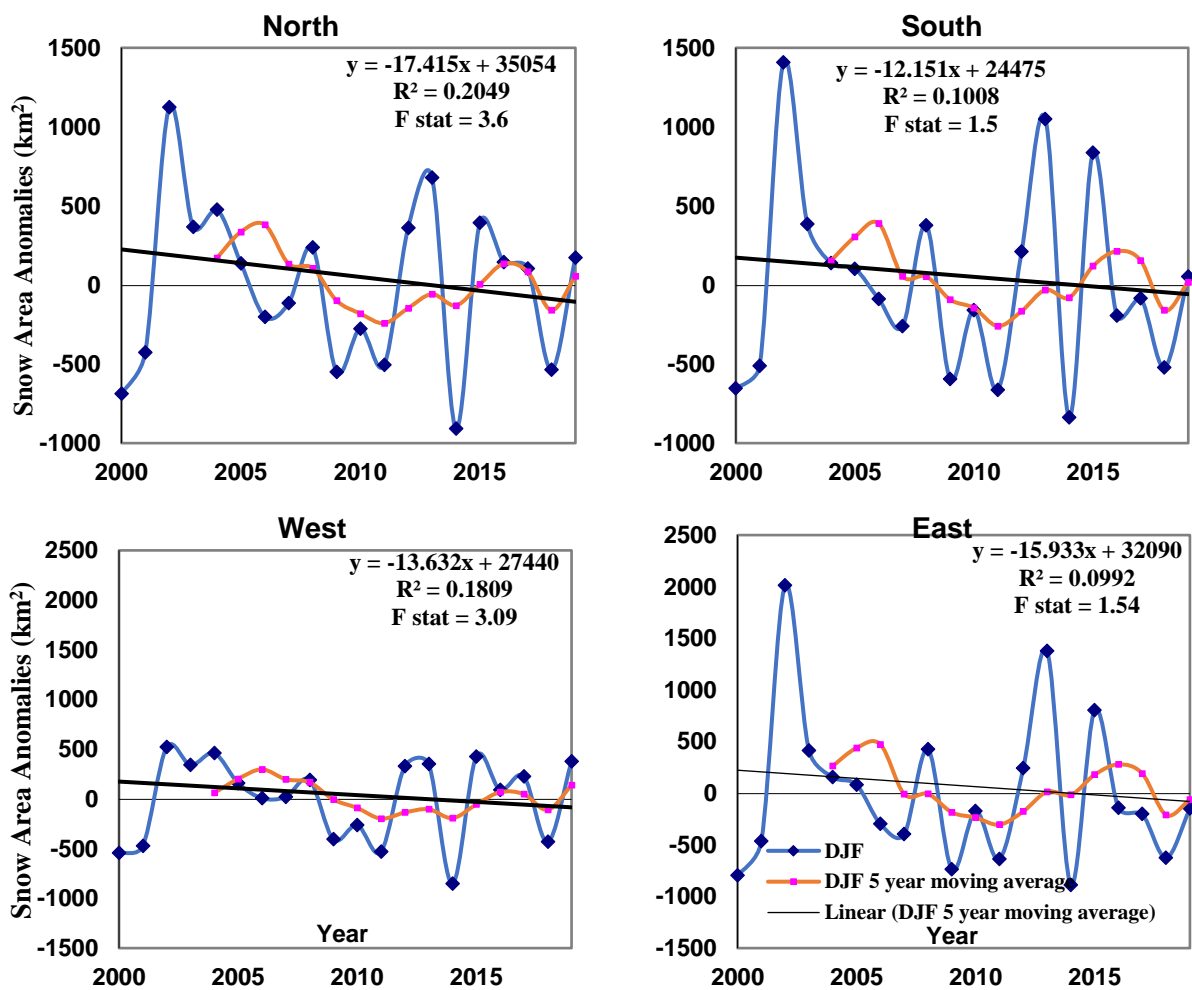


Figure 19. Winter average Snow Area Anomalies km² over the north, south, east, and west areas

During the Spring (MAM) season, a negative trend dominated the north, south, and west basins while the east basin showed a positive trend, the northern basin showed a decreasing slope of 0.67 km²/year. For the southern basin, the negative slope was about 0.17 km²/year. For the western basin, the negative slope was about 2.3 km²/year. For the eastern basin, the positive slope was about 1.5 km²/year (Figure 20). The southern watershed showed no significance while remaining watersheds showed significance with only the median crossing and turning point test with a 2010-year mean change for the east, 2005-year mean change for the north and 2012-year mean change for the western watersheds. No significance with the Mann-Kendall test was observed (Table 8).

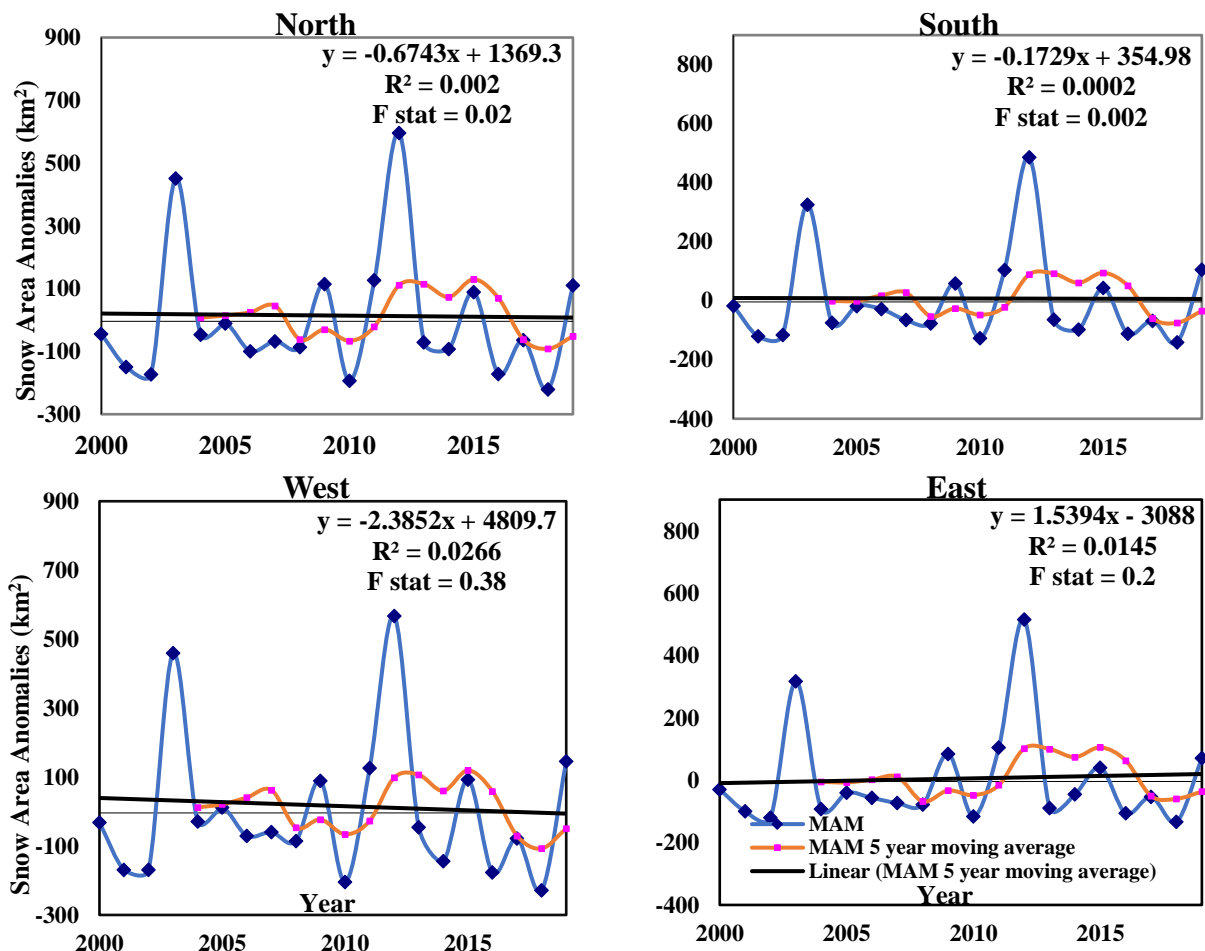


Figure 20. Spring average Snow Area Anomalies km² over the north, south, east, and west areas

Table 9. MODIS seasonal trend results for the snow cover area anomalies over the north, east, west, and south basins.

Year of change	Basin	Season	Statistical test	Test statistic	Critical Value at 0.1	Critical Value at 0.05	Critical Value at 0.01	Result
2010	East	MAM	Median Crossing	2.065	1.563	1.862	2.447	<i>S (0.05)</i>
2007	East	SON	Turning Point	-3.051	1.481	1.764	2.318	<i>S (0.01)</i>
2005	North	MAM	Turning Point	1.668	1.563	1.862	2.447	<i>S (0.1)</i>
2005	North	SON	Median Crossing	1.886	1.481	1.764	2.318	<i>S (0.05)</i>
2005	South	SON	Mann-Kendall	-1.714	1.481	1.764	2.318	<i>S (0.1)</i>
2005	South	SON	Spearman's Rho	-1.92	1.481	1.764	2.318	<i>S (0.05)</i>
2012	West	MAM	Turning Point	1.668	1.563	1.862	2.447	<i>S (0.1)</i>
2005	West	SON	Median Crossing	1.886	1.481	1.764	2.318	<i>S (0.05)</i>

During the Fall (SON) season, a negative trend dominated all basins, showing the highest value in the northern basin with a decrease of 6.3 km²/year. For the southern basin, the negative slope was about 3.2 km²/year. For the western basin, the negative slope was about 4.4 km²/year. For the eastern basin, the negative slope was about 5.1 km²/year (Figure 21). All watershed showed significance with different tests, while only the Southern watershed showed significance with the Mann-Kendall test at 0.1 with a 2005-year mean change (Table 10).

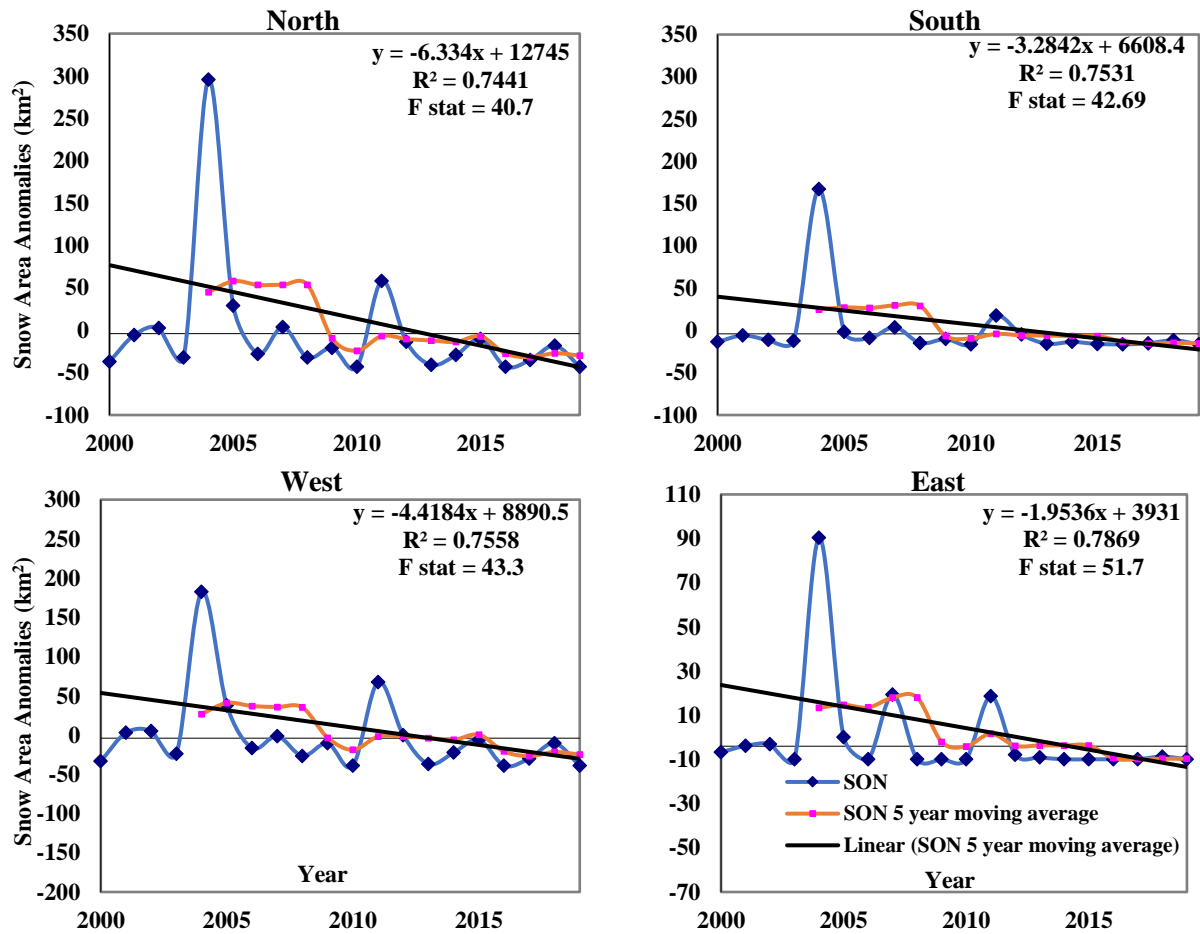


Figure 21. Fall average Snow Area Anomalies km² over the north, south, east, and west areas

A percent mean change analysis was done on the annual snow cover area for each watershed; the Landsat analysis showed a 29% change with an average area of 1013 km² for the whole Lebanese area (Table 10). We also observed a higher % mean change for all the other watersheds peaking with the eastern at 31.4%, followed by the northern 30.1%, and around 27.6% and 27% for the southern and western watersheds respectively (Table 10).

Table 10. Snow Area % mean Change for the North, South, West, East and the whole Lebanese area using the Landsat dataset between 1985 and 2019 snow seasons

<i>Area</i>	<i>Mean Area (km²)</i>	<i>Year of Change</i>	<i>1st Period Mean</i>	<i>2nd Period Mean</i>	<i>Mean % change</i>
<i>Lebanon</i>	1012.97	2005	1185.93	840.01	-29.16
<i>North</i>	628.17	2005	739.57	516.76	-30.12
<i>South</i>	384.8	2005	446.35	323.25	-27.57
<i>West</i>	516.45	2005	596.79	436.11	-26.92
<i>East</i>	496.52	2005	589.13	403.9	-31.44

G. Snow Density vs. Snow Albedo

Albedo retrieved from the Landsat dataset showed good correlation with the field measured snow density measurement during the 2015-2016 snow season (Fayad, Gascoin, Faour, Fanise, et al., 2017) with a 0.51 R² coefficient using the polynomial trendline raised to the second-order (Figure 22). While the albedo retrieved from the MODIS dataset showed a lower R² coefficient of about 0.32 using the same field measurement, which may be due to the larger pixel size of MODIS (Figure 23). This method will allow for a near real-time density estimation using either Landsat or daily MODIS albedo measurements. The estimated density with the combination of remotely sensed snow area and either remotely sensed or field measurements of snow depth will allow for SWE estimation.

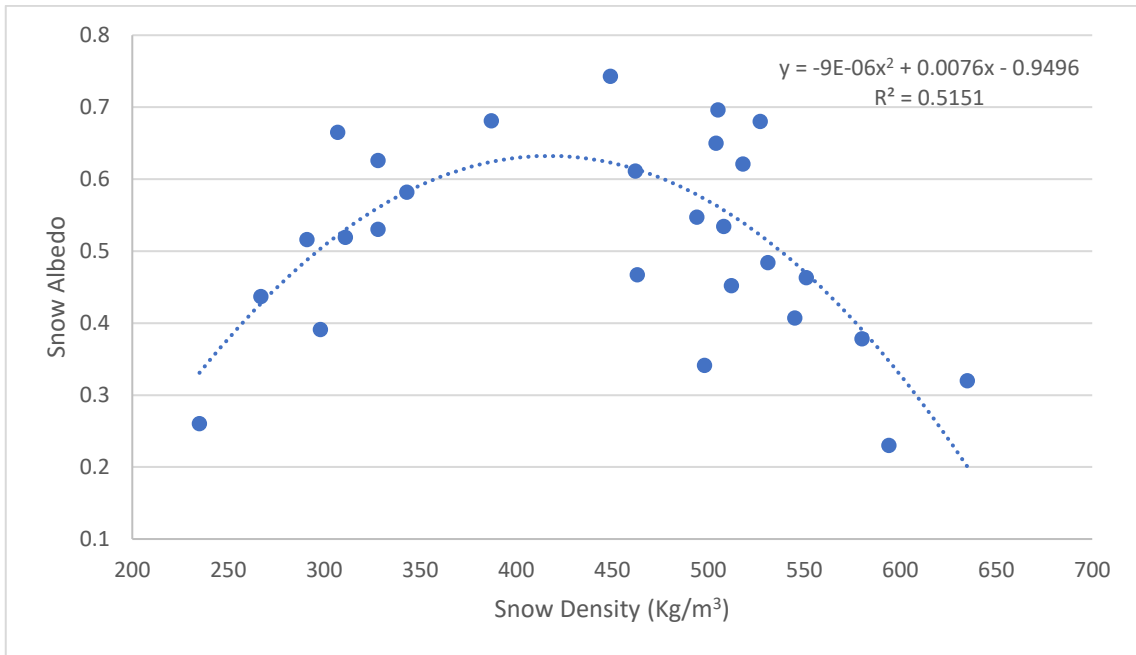


Figure 22. Landsat Albedo vs. Field Snow Density observations (Fayad et al., 2017)

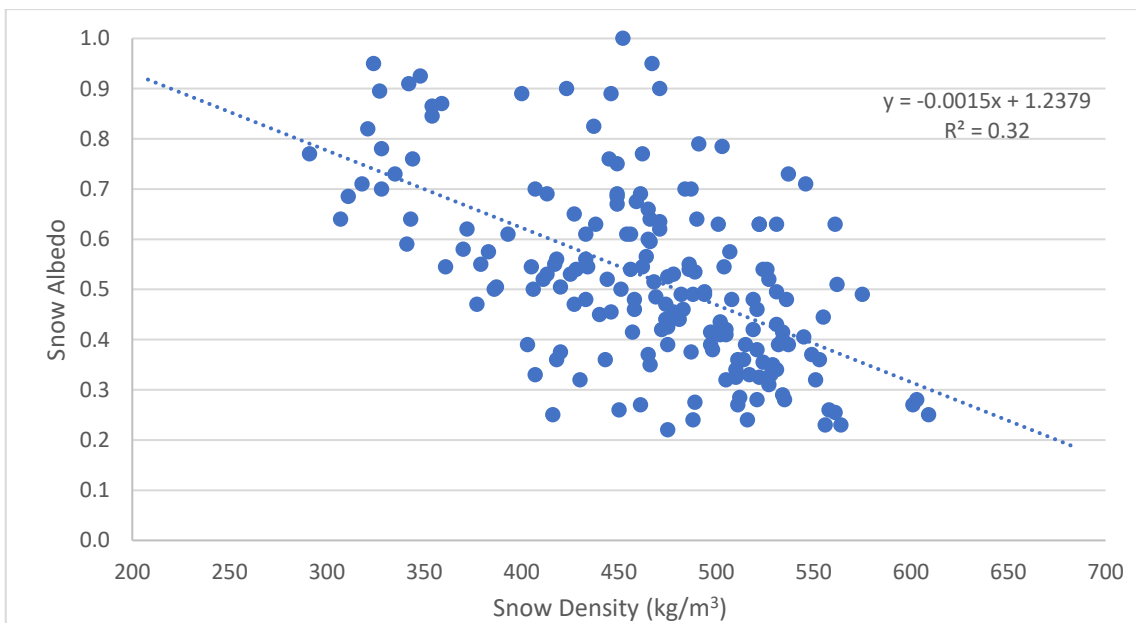


Figure 23. MODIS Albedo vs. Field Snow Density observations (Fayad et al., 2017)

H. Snow Area vs. Temperature vs. Precipitation

The comparison between the annual snow area with the average annual temperature (Figure 24) and the total annual precipitation showed evidence of the previously stated hypothesis that the climate is moving from a snow-dominated to eventually a rain dominated climate, which is shown by the average annual temperature increase of about 1 degree since 1985 for all the basins (figure 25) with an increase of the total annual precipitation of about 1.29 mm per year (figure 26).

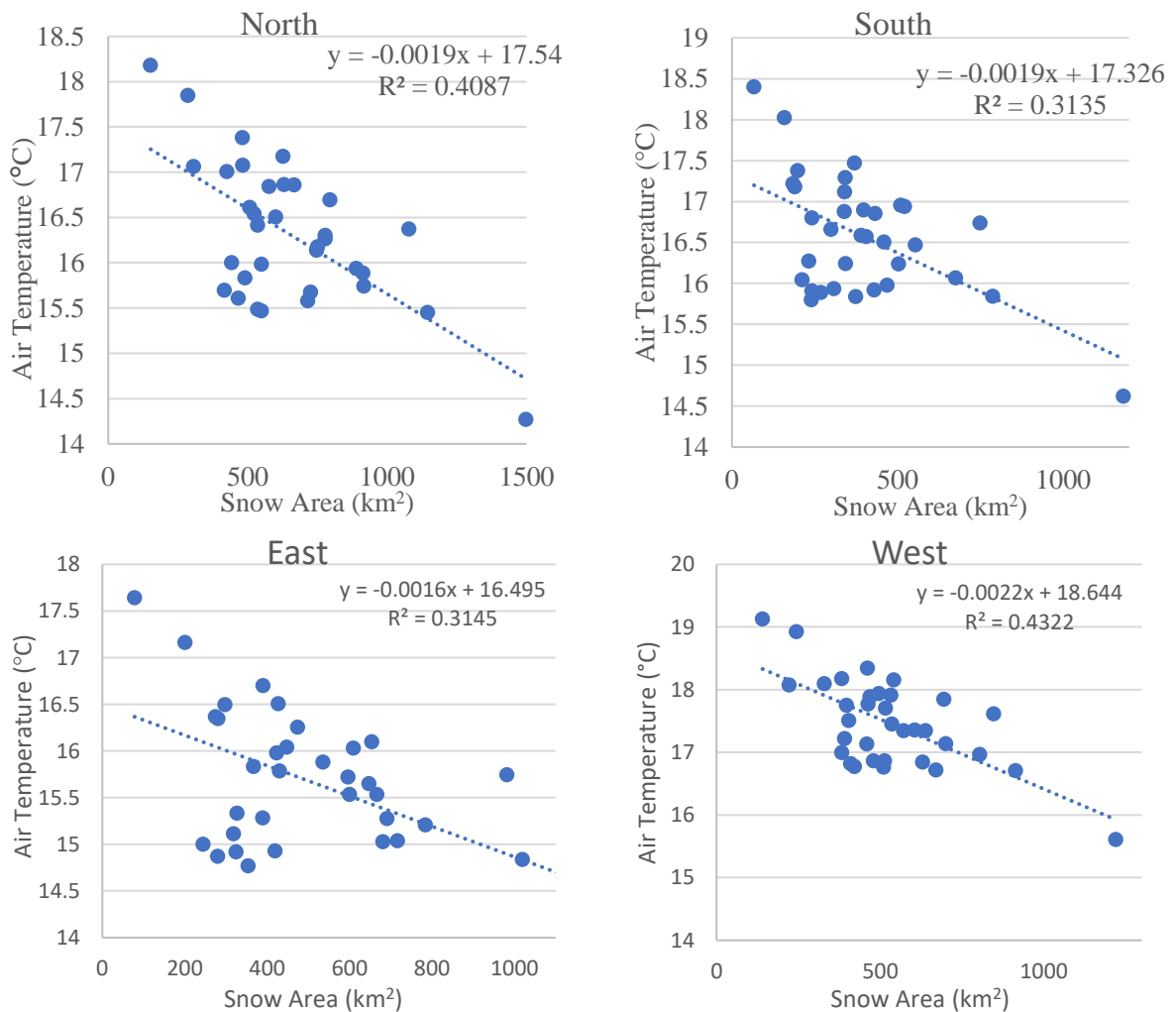


Figure 24. Annual Average Temperature vs. Annual Snow Area for the North, South, East, West basins

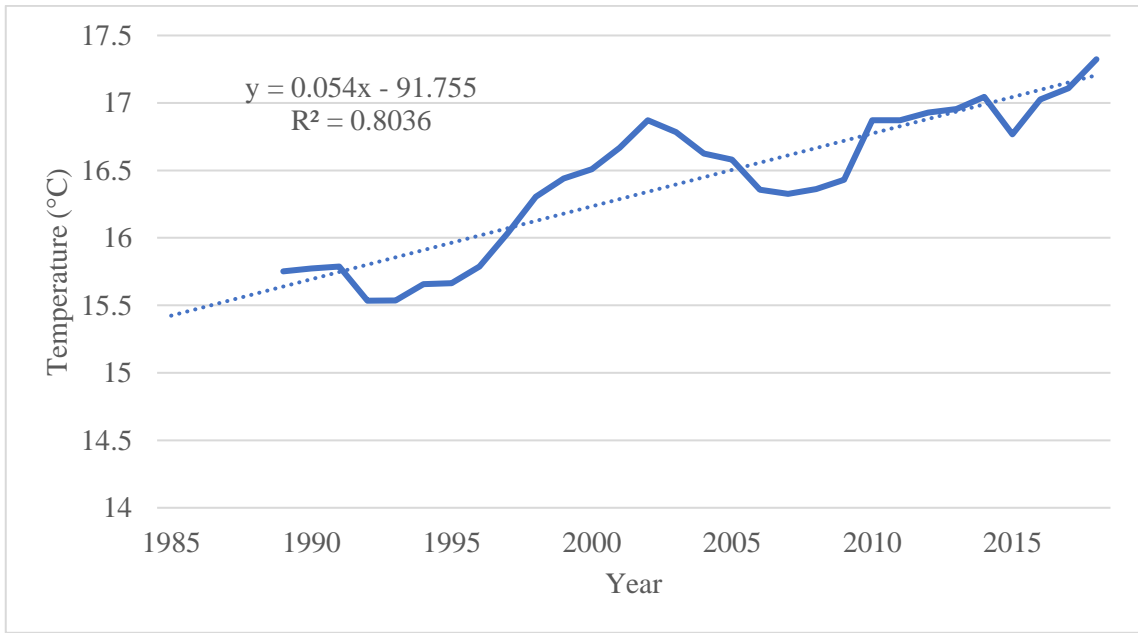


Figure 25. 5-year moving average for the annual air Temperature °C over the full area between 1985 and 2019

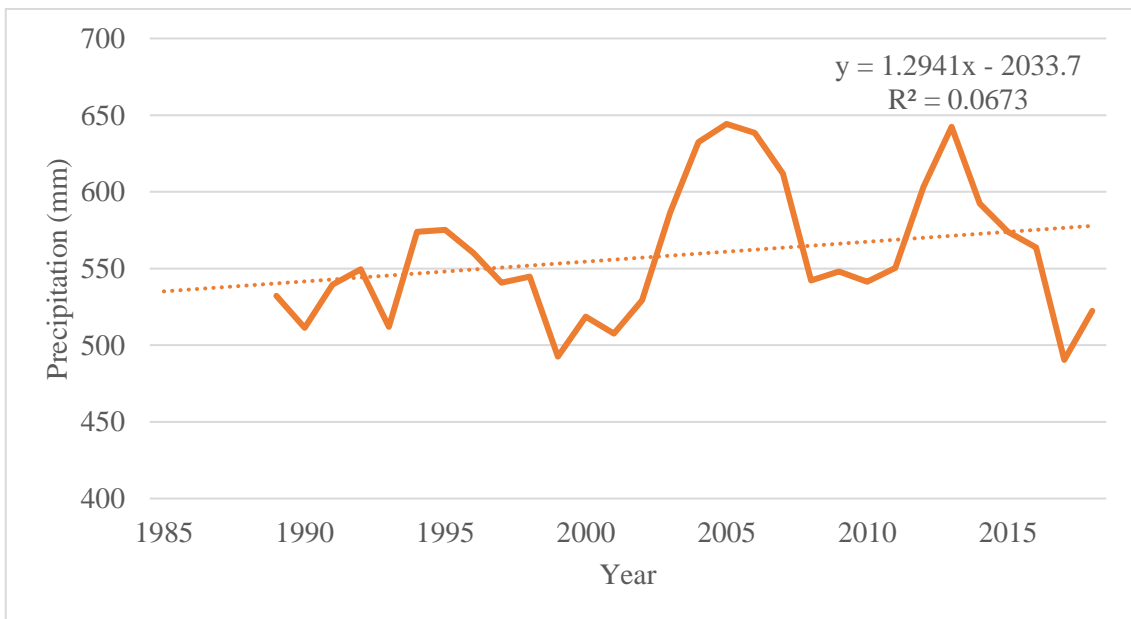


Figure 26. 5-year moving average for the annual precipitation mm over the full area between 1985 and 2019

For the temperature analysis, all the basins showed significance for the decreasing trend using all 12 significance tests (Table 16), while precipitation analysis did not show any significance. The correlation between the annual snow area and the annual average temperature showed good correlation, over the four basins the coefficient of correlation r was higher than 0.55 and a negative value showing that they are inversely proportional which indicates that the increase in temperature due to global warming is directly affecting the snow area (Table 11). Correlation was also done on a seasonal time basis, which showed great results when comparing the average seasonal temperatures to the average seasonal snow area, with the lowest coefficient of correlating for the southern watershed with a coefficient of 0.76 and negative correlation values for all basins showing the inverse proportionality of the temperature and snow area (Table 12). The same analysis was done on each season separately apart from the summer season, seeing as snow area is not significant during that season. The main idea was that the increase in average temperatures over the years is causing faster snowmelt which means a decrease in snow area during the winter and especially during the spring seasons. The results for the winter season showed a good negative correlation between the average snow area and the average temperature (Table 13), which is also the case for the spring season (Table 14), while the fall season showed a weak negative correlation (Table 15). The Strong correlation during the winter and spring seasons shows clear proof of the adverse effects the increase in average temperature is having on the average snow area since 1985. No correlation between the snow area and the rainfall was observed, indicating that the decrease in snow area is mainly due to the increase in temperature.

Table 11. Results of correlation analysis between Annual Temperature and Annual snow Area

<i>Annual</i>	<i>North</i>	<i>South</i>	<i>East</i>	<i>West</i>
<i>Coefficient r:</i>	-0.63	-0.55	-0.56	-0.65
<i>N:</i>	34	34	34	34
<i>T statistic:</i>	-4.70	-3.82	-3.83	-4.93
<i>DF:</i>	32	32	32	32
<i>p value:</i>	4.7E-05	0.00057	0.00056	2.4E-05

Table 12. Results of correlation analysis between Seasonal Temperature and Seasonal snow Area (All Seasons)

<i>All Seasons</i>	<i>North</i>	<i>South</i>	<i>West</i>	<i>East</i>	<i>Lebanon</i>
<i>Coefficient r:</i>	-0.84	-0.76	-0.85	-0.77	-0.82
<i>N:</i>	138	138	138	138	138
<i>T statistic:</i>	-18.34	-14.06	-18.87	-14.43	-16.74
<i>DF:</i>	136	136	136	136	136
<i>p value:</i>	1.35E-38	2.7E-28	8.14E-40	3.28E-29	7.53E-35

Table 13. Results of correlation analysis between the Winter Temperature and Winter snow Area

<i>Winter</i>	<i>North</i>	<i>South</i>	<i>West</i>	<i>East</i>	<i>Lebanon</i>
<i>Coefficient r:</i>	-0.73	-0.67	-0.76	-0.66	-0.71
<i>N:</i>	34	34	34	34	34
<i>T statistic:</i>	-6.07	-5.23	-6.68	-5.04	-5.83
<i>DF:</i>	32	32	32	32	32
<i>p value:</i>	8.71E-07	9.89E-06	1.53E-07	1.75E-05	1.75E-06

Table 14. Results of correlation analysis between the Spring Temperature and Spring snow Area

Spring	North	South	West	East	Lebanon
Coefficient r:	-0.69	-0.59	-0.67	-0.59	-0.66
N:	35	35	35	35	35
T statistic:	-5.61	-4.24	-5.29	-4.29	-5.11
DF:	33	33	33	33	33
p value:	3.01E-06	0.0001	7.81E-06	0.0001	1.33E-05

Table 15. Results of correlation analysis between the Fall Temperature and Fall snow Area

Fall	North	South	West	East	Total Area
Coefficient r:	-0.35	-0.19	-0.37	-0.24	-0.29
N:	34	34	34	34	34
T statistic:	-2.15	-1.11	-2.25	-1.45	-1.77
DF:	32	32	32	32	32
p value:	0.03	0.27	0.03	0.15	0.08

Table 16. Statistical significance of the 5-year moving average annual air Temperature trend analysis

Year of change	Statistical test	Test statistic	Critical Value at 0.1	Critical Value at 0.05	Critical Value at 0.01	Result
1997	Mann-Kendall	4.833	1.645	1.96	2.576	S (0.01)
1997	Spearman's Rho	4.454	1.645	1.96	2.576	S (0.01)
1997	Linear regression	6.204	1.694	2.038	2.741	S (0.01)
1997	Cusum	11	7.114	7.93	9.504	S (0.01)
1997	Cumulative deviation	2.056	1.124	1.248	1.476	S (0.01)
1997	Worsley likelihood	5.965	2.876	3.206	3.868	S (0.01)
1997	Rank Sum	-4.126	1.645	1.96	2.576	S (0.01)
1997	Student's t	-2.727	1.693	2.036	2.736	S (0.05)
1997	Median Crossing	2.611	1.645	1.96	2.576	S (0.01)
1997	Turning Point	-1.812	1.645	1.96	2.576	S (0.1)
1997	Rank Difference	-4.368	1.645	1.96	2.576	S (0.01)
1997	Auto Correlation	3.174	1.645	1.96	2.576	S (0.01)

I. Sentinel-1 vs. Field measured snow depth

Snow depth retrieved from the Sentinel 1 methodology previously stated did not show correlation with the snow depth measurements retrieved from a combination of 3 automatic weather stations situated along the western slopes of Mount Lebanon (Fayad, Gascoin, Faour, Fanise, et al., 2017). Which agrees with (Lievens et al., 2019) findings that stated the importance of applying this method on large scale analysis and not restrict it to point/small watershed analysis (Figure 27). The retrieval of remotely sensed snow depth from Sentinel-1 will allow for retrieval of snow depth from inaccessible/unreachable areas, near real-time snow depth estimations will allow for better SWE calculation and forecasting in remote areas.

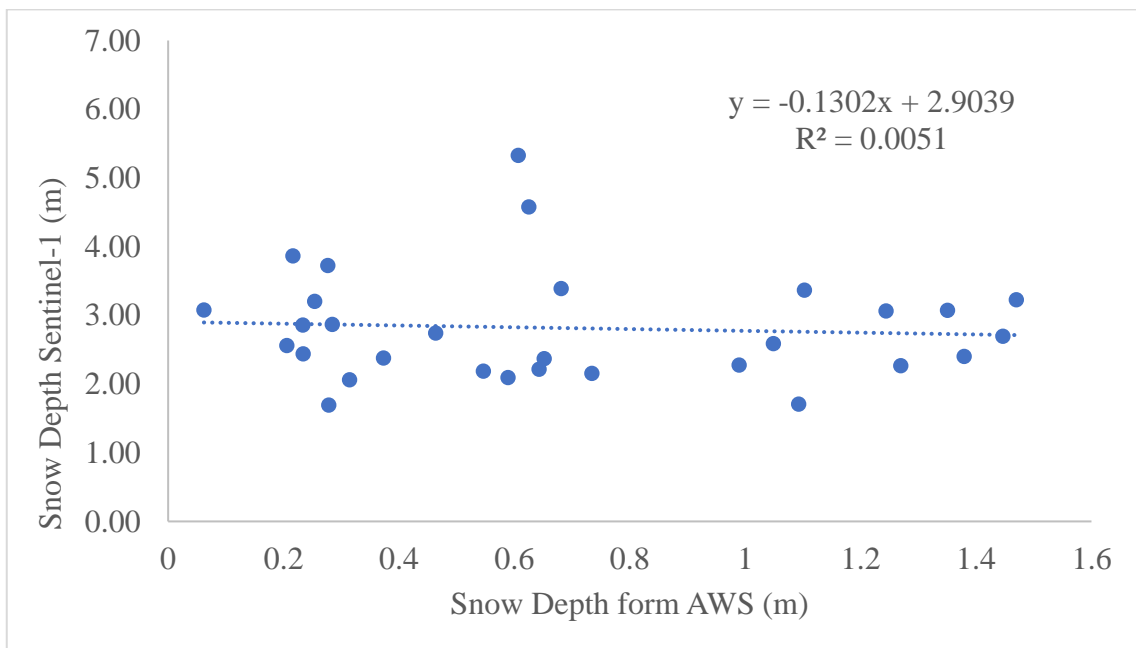


Figure 27. Comparison between Snow depth retrieved from Sentinel-1 and Snow depth retrieved from an Automatic weather station's Acoustic sensor between 2015 and 2016 (Fayad et al., 2017)

J. River vs. Snow Area

A comparison between the monthly snow area and the monthly streamflow for the Litany River taken at Jib Jannine (Figure 28) showed good significance with a high coefficient of R (Table 17). A seasonal correlation between the Litany streamflow and Snow area showed a strong correlation during the winter, spring and peaking during the summer season, which shows the effect of snowmelt on the flow of the litany river (Table 17). This comparison will allow for backward retrieval of SWE for the Litany watershed. The analysis of the annual Litany streamflow showed a decreasing trend since 1984 of about 2.5 Mm³/year, but no significance was shown using the statistical tests previously discussed. Trend analysis showed a 2005 year mean change for the snow Area over the Litani watershed when compared to the insignificant Litani Precipitation (Figure 29) and the river flow. This comparison shows that the decrease in the Litani river flow is mainly due to the decrease in the Snow Area decrease (Table 18)

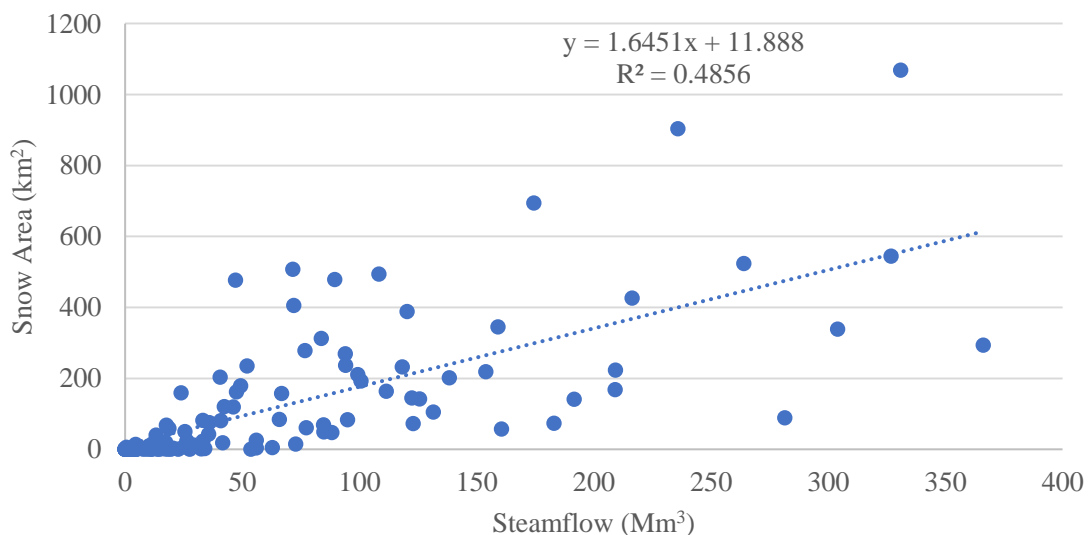


Figure 28. Seasonal Snow Area vs. Streamflow for the Litany river at Jib Jannine

Table 17. Significance of the monthly and seasonal Litani Flow vs. Snow Area

	Monthly	Winter	Spring	Summer	Fall
Coefficient r:	0.66	0.62	0.64	0.90	0.28
N:	327	28	27	27	27
T statistic:	16.08	4.12	4.21	10.93	1.46
DF:	325	26	25	25	25
p value:	3.22E-43	0.0003	0.0002	5.09E-11	0.15

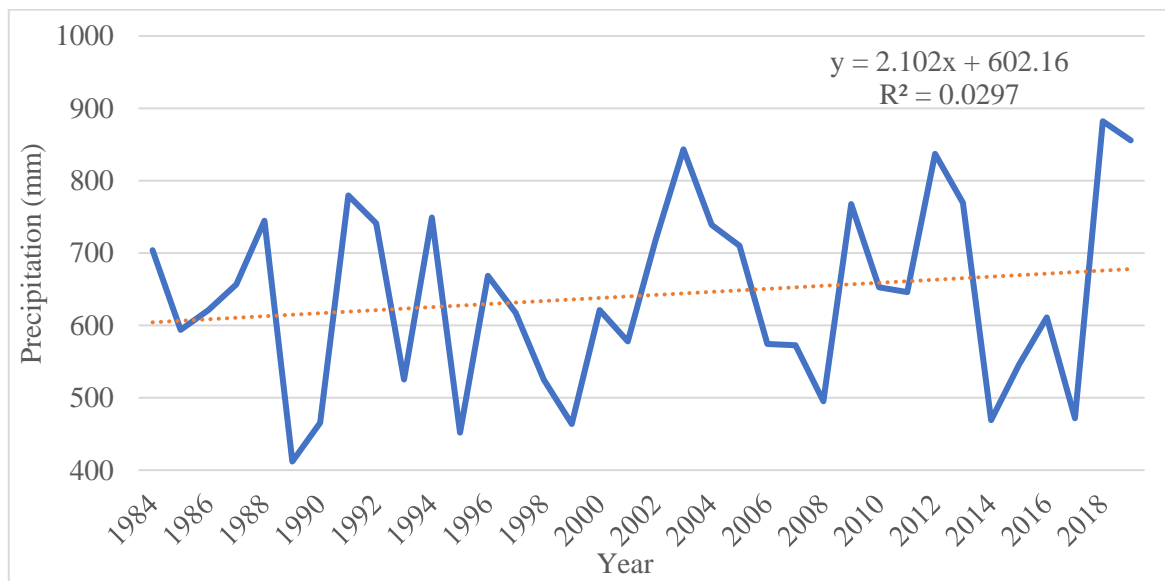


Figure 29. Annual precipitation mm over the Litani watershed between 1985 and 2019

Table 18. Upper Litani Flow (Mm^3), Snow Area (Km^2), and Precipitation (mm) 2005 year mean change and % change

	1985-2005	2005-2011	% Change
Upper Litani Flow (Mm^3)	303.6	207.6	-32
Snow Area (km^2)	137.7	98.5	-28
Precipitation (mm)	633.1	631.1	-0.32

K. Discussion

The snow cover days for both Landsat since 1985 and MODIS since 2000 agreed that there is a decrease in the total days of snow cover presence over the four main basins and the whole area. Landsat is more sensitive due to the higher resolution of 30 meters compared to the MODIS resolution of 500 meters, where on average, over the overlap period between 2000 till 2018, Landsat detected about 23% more days per year with snow cover for the whole area than MODIS did. Both Landsat and MODIS agreed on the decreasing snow cover days trend, where MODIS showed a more significant decreasing trend of about two days than Landsat did.

Since 1985 snow cover area peaked during the 1992 winter season with an area of around 2680 km². Since then, only the 2002 snow season was able to surpass half of that area, with an area of around 1829 km². Both the Landsat and MODIS analysis for snow cover agreed on the negative trend. The seasonal analysis showed more in-depth results about the distribution of the decreasing trend between the seasons, not taking into consideration the magnitude of the trends, both datasets agreed on the decreasing trend for all seasons, which shows that through the years, during the fall seasons the snowfall is being set back, during the winter season a smaller area is being covered by snow, and during the spring season, the snow is melting faster which will affect water availability during the late summer months for agricultural, domestic and industrial needs. These results are reaffirmed by the correlation analysis of the seasonal snow area with the seasonal average temperature over the four main basins and the whole area. This correlation showed that the increase in average temperature since 1985 has been affecting the snow area. Some disagreements appeared between the datasets where the MODIS dataset underrated the spring snow area trend magnitude, Which is also proved

by the comparison of the Litani streamflow with the snow area and precipitation that showed that the decreasing % mean change is mainly due to the decrease in snow area and while the precipitation showed no trend. For the Albedo estimation from both Landsat and MODIS had good agreement with snow density readings over the Kelb, Ibrahim, Abo Ali basin, taking into consideration that the Landsat Albedo measurements had a higher R2 than the MODIS Albedo when compared with the field data, which may be due to the larger Landsat resolution. Snow depth estimation did not yield good results due to effect of topography and the fact that the method that uses Sentinel-1 for snow depth retrieval should only be applied to large areas with a high density of snow depth readings where in our case were restricted to three weather stations with data between 2014 and 2016. Other proven methods for snow depth retrieval use the 25km microwave datasets which would only work on large flat terrain.

CHAPTER V

CONCLUSION AND RECOMMENDATIONS

Remote sensing of snow continues to contribute to our understanding of the Earth's system processes. The MODIS, Landsat, Sentinel snow retrieval are valuable because they provide high-resolution snow cover area, snow cover days, snow density, and snow depth estimations under cloudy and cloud-free conditions using different algorithms. Future work could focus on Snow depth estimation using high-resolution imagery for small basins.

This paper presents the first time series analysis of snow cover area and snow cover days for the past 35 years, while also analyzing the retrieval of snow density from Albedo and snow depth from Sentinel-1. This time series analysis has revealed the effect of Global warming on snow cover in the Levant region, where the snow cover area and snow cover days analysis between 1985 and 2019 and its correlation with temperature proved the decreasing trend of snow presence with the increasing average temperatures over the Lebanese mountains. Snowfall constitutes a significant fraction of the total precipitation and water availability. The effect of climate change will significantly decrease the groundwater recharge and surface water availability during the dry months for agriculture and domestic needs. Even though snow depth analysis with Sentinel-1 did not yield good results, the use of the method has been proved in literature, with the combination of the correlated Albedo and snow density on a larger area that will yield real-time SWE estimations.

For future studies, it is recommended to research further improvement regarding snow depth retrieval at a higher spatial resolution, which might mitigate the effect of

topography and study the effect of wet snow on the Sentinel-1 C band. Retrieve snow area from Sentinel-2 product as it has a higher spatial resolution and a smaller temporal resolution. Improve cloud detection algorithms. Utilize the above to derive the impact of climate change on SWE and river flow in Lebanese catchments

APPENDIX I

STATISTICAL SIGNIFICANCE

Table 19. Statistical results for the Annual Landsat 5-year moving average Snow Area for all basins

<i>Annual</i>	<i>North</i>	<i>South</i>	<i>East</i>	<i>West</i>	<i>NorthWest</i>	<i>NorthEast</i>	<i>SouthWest</i>	<i>SouthEast</i>	<i>WestWest</i>	<i>WestEast</i>	<i>EastWest</i>	<i>EastEast</i>
<i>Slope</i>	-9.80	-5.10	-7.46	-7.44	-5.38	-4.42	-2.06	-3.04	-4.95	-2.50	-2.89	-4.57
<i>St. error of the slope</i>	2.13	1.93	2.36	1.69	1.02	1.13	0.69	1.25	0.96	0.74	0.76	1.61
<i>R²</i>	0.42	0.19	0.26	0.40	0.49	0.35	0.24	0.17	0.48	0.28	0.33	0.22
<i>F statistics</i>	21.19	6.99	9.99	19.31	28.08	15.31	9.01	5.93	26.85	11.28	14.44	8.04
<i>Regression sum of squares</i>	238128.85	64628.07	137987.23	137447.15	71849.13	48372.55	10545.60	22960.96	60723.27	15454.90	20662.97	51859.23
<i>Intercept</i>	19641.61	10234.01	14952.94	14922.68	10788.19	8853.42	4134.49	6099.52	9917.54	5005.14	5786.19	9166.99
<i>St. error of the intercept</i>	4265.64	3870.42	4729.23	3394.99	2035.75	2262.17	1376.92	2504.04	1913.91	1489.44	1522.24	3232.03
<i>St. error of the Y</i>	106.00	96.18	117.52	84.37	50.59	56.21	34.22	62.23	47.56	37.01	37.83	80.32
<i>Degrees of freedom</i>	29.00	29.00	29.00	29.00	29.00	29.00	29.00	29.00	29.00	29.00	29.00	29.00
<i>Residual sum of squares</i>	325847.07	268263.99	400522.40	206406.58	74215.51	91642.60	33952.05	112286.73	65597.64	39727.47	41496.27	187066.58

Table 20. Statistical results for the Winter Landsat 5-year moving average Snow Area for all basins

<i>DJF</i>	<i>North</i>	<i>South</i>	<i>East</i>	<i>West</i>	<i>NorthWest</i>	<i>NorthEast</i>	<i>SouthWest</i>	<i>SouthEast</i>	<i>WestWest</i>	<i>WestEast</i>	<i>EastWest</i>	<i>EastEast</i>
<i>Slope</i>	-25.93	-14.13	-20.80	-19.26	-13.47	-12.46	-5.79	-8.34	-12.46	-6.80	-8.60	-12.20
<i>St. error of the slope</i>	7.16	6.89	8.21	5.85	3.49	3.76	2.38	4.54	3.23	2.63	2.56	5.70
<i>R²</i>	0.31	0.13	0.18	0.27	0.34	0.27	0.17	0.10	0.34	0.19	0.28	0.14
<i>F statistics</i>	13.11	4.21	6.42	10.85	14.91	10.98	5.95	3.38	14.92	6.68	11.26	4.59
<i>Regression sum of squares</i>	1667264.99	495400.52	1073317.28	919801.51	449694.53	385185.93	83215.03	172537.87	384950.95	114662.61	183466.53	369275.40
<i>Intercept</i>	51988.90	28343.68	41717.62	38614.96	26997.47	24991.43	11617.49	16726.19	24977.47	13637.48	17246.09	24471.53
<i>St. error of the intercept</i>	14349.17	13807.34	16450.02	11716.44	6989.63	7535.64	4760.39	9091.20	6464.91	5270.35	5137.70	11415.36
<i>St. error of the Y</i>	356.57	343.11	408.78	291.15	173.69	187.26	118.30	225.92	160.65	130.97	127.67	283.67
<i>Degrees of freedom</i>	29.00	29.00	29.00	29.00	29.00	29.00	29.00	29.00	29.00	29.00	29.00	29.00
<i>Residual sum of squares</i>	3687218.62	3414016.64	4845944.52	2458311.69	874891.32	1016918.95	405817.90	1480090.81	748462.78	497422.02	472696.89	2333591.15

Table 21. Statistical results for the Spring Landsat 5-year moving average Snow Area for all basins

<i>MAM</i>	<i>North</i>	<i>South</i>	<i>East</i>	<i>West</i>	<i>NorthWest</i>	<i>NorthEast</i>	<i>SouthWest</i>	<i>SouthEast</i>	<i>WestWest</i>	<i>WestEast</i>	<i>EastWest</i>	<i>EastEast</i>
<i>Slope</i>	-8.76	-5.10	-6.22	-7.64	-5.55	-3.21	-2.09	-3.01	-5.35	-2.29	-1.98	-4.24
<i>St. error of the slope</i>	1.85	1.52	1.74	1.74	1.13	0.87	0.62	0.93	1.13	0.64	0.59	1.18
<i>R²</i>	0.44	0.28	0.31	0.40	0.45	0.32	0.28	0.26	0.44	0.30	0.28	0.31
<i>F statistics</i>	22.34	11.18	12.78	19.23	23.94	13.55	11.30	10.44	22.47	12.66	11.38	12.85
<i>Regression sum of squares</i>	190287.46	64436.15	95870.51	144728.99	76338.03	25576.36	10844.98	22411.14	70997.45	12991.25	9717.11	44543.89
<i>Intercept</i>	17549.85	10214.99	12454.87	15309.98	11118.32	6431.53	4191.66	6023.33	10722.38	4587.61	3965.08	8489.79
<i>St. error of the intercept</i>	3713.61	3054.93	3485.50	3490.87	2272.53	1748.07	1246.65	1864.88	2261.94	1289.02	1175.92	2369.72
<i>St. error of the Y</i>	92.28	75.91	86.61	86.75	56.47	43.44	30.98	46.34	56.21	32.03	29.22	58.89
<i>Degrees of freedom</i>	29.00	29.00	29.00	29.00	29.00	29.00	29.00	29.00	29.00	29.00	29.00	29.00
<i>Residual sum of squares</i>	246967.17	167127.83	217558.46	218229.51	92483.60	54722.05	27831.18	62279.99	91623.61	29755.48	24762.87	100562.95

Table 22. Statistical results for the Summer Landsat 5-year moving average Snow Area for all basins

JJA	North	South	East	West	NorthWest	NorthEast	SouthWest	SouthEast	WestWest	WestEast	EastWest	EastEast
Slope	-0.07	-0.06	-0.03	-0.10	-0.06	-0.01	-0.04	-0.02	-0.06	-0.04	0	-0.03
St. error of the slope	0.03	0.02	0.01	0.05	0.03	0.00	0.01	0.01	0.03	0.01	0	0.01
R ²	0.11	0.25	0.41	0.13	0.11	0.14	0.18	0.43	0.10	0.20	0.16	0.41
F statistics	3.76	9.46	20.35	4.33	3.48	4.76	6.17	21.62	3.18	7.37	5.62	20.54
Regression sum of squares	11.08	9.06	2.08	24.00	9.47	0.06	3.32	1.42	8.51	3.92	0.01	1.81
Intercept	133.57	120.91	57.90	196.57	123.49	10.08	73.08	47.83	116.99	79.58	4.82	54.07
St. error of the intercept	69.04	39.39	12.85	94.77	66.37	4.63	29.50	10.30	65.82	29.36	2.04	11.94
St. error of the Y	1.72	0.98	0.32	2.36	1.65	0.11	0.73	0.26	1.64	0.73	0.05	0.30
Degrees of freedom	29.00	29.00	29.00	29.00	29.00	29.00	29.00	29.00	29.00	29.00	29.00	29.00
Residual sum of squares	85.37	27.78	2.96	160.85	78.88	0.38	15.59	1.90	77.58	15.44	0.07	2.55

Table 23. Statistical results for the Fall Landsat 5-year moving average Snow Area for all basins

SON	North	South	East	West	NorthWest	NorthEast	SouthWest	SouthEast	WestWest	WestEast	EastWest	EastEast
Slope	-5.06	-1.51	-3.30	-3.26	-2.81	-2.25	-0.46	-1.05	-2.22	-1.04	-1.14	-2.17
St. error of the slope	1.43	0.77	1.38	0.85	0.60	0.88	0.27	0.52	0.50	0.37	0.45	0.92
R ²	0.30	0.12	0.17	0.34	0.43	0.18	0.09	0.12	0.41	0.22	0.18	0.16
F statistics	12.54	3.87	5.73	14.66	22.03	6.55	2.91	4.14	19.85	8.09	6.25	5.48
Regression sum of squares	63414.67	5651.56	27032.27	26433.77	19573.88	12525.19	514.29	2756.14	12244.21	2696.84	3201.46	11628.06
Intercept	10139.12	3027.85	6622.16	6544.81	5631.56	4507.56	913.26	2114.59	4453.72	2091.09	2278.90	4343.25
St. error of the intercept	2861.59	1538.25	2763.14	1708.84	1199.63	1760.11	535.20	1038.17	999.35	734.56	910.91	1853.69
St. error of the Y	71.11	38.23	68.66	42.46	29.81	43.74	13.30	25.80	24.83	18.25	22.64	46.06
Degrees of freedom	29.00	29.00	29.00	29.00	29.00	29.00	29.00	29.00	29.00	29.00	29.00	29.00
Residual sum of squares	146642.69	42374.07	136726.44	52293.42	25771.32	55478.36	5129.62	19301.00	17884.59	9662.73	14859.21	61534.98

Table 24. Statistical results for the Annual MODIS 5-year moving average Snow Area for all basins

<i>Annual</i>	<i>North</i>	<i>South</i>	<i>East</i>	<i>West</i>	<i>NorthWest</i>	<i>NorthEast</i>	<i>SouthWest</i>	<i>SouthEast</i>	<i>WestWest</i>	<i>WestEast</i>	<i>EastWest</i>	<i>EastEast</i>
<i>Slope</i>	-4.98	-3.16	-4.23	-3.91	-2.84	-2.14	-1.06	-2.10	-2.30	-1.60	-1.05	-3.18
<i>St. error of the slope</i>	2.87	2.75	3.58	2.45	1.62	1.58	0.85	2.03	1.48	1.03	1.26	2.35
<i>R²</i>	0.18	0.09	0.09	0.15	0.18	0.12	0.10	0.07	0.15	0.15	0.05	0.12
<i>F statistics</i>	3.02	1.32	1.40	2.54	3.07	1.84	1.57	1.06	2.43	2.39	0.70	1.82
<i>Regression sum of squares</i>	8426.78	3393.99	6088.79	5186.66	2747.45	1550.34	384.25	1494.09	1805.94	871.52	376.03	3436.99
<i>Intercept</i>	10018.14	6361.16	8521.04	7857.57	5719.34	4298.03	2138.22	4222.70	4636.98	3220.52	2117.23	6402.36
<i>St. error of the intercept</i>	5766.41	5535.09	7206.44	4926.85	3261.25	3170.73	1708.43	4088.58	2976.21	2081.86	2525.13	4736.74
<i>St. error of the Y</i>	52.86	50.74	66.06	45.16	29.90	29.07	15.66	37.48	27.28	19.08	23.15	43.42
<i>Degrees of freedom</i>	14.00	14.00	14.00	14.00	14.00	14.00	14.00	14.00	14.00	14.00	14.00	14.00
<i>Residual sum of squares</i>	39117.90	36042.42	61095.09	28556.39	12512.20	11827.26	3433.68	19665.71	10420.56	5098.79	7501.23	26395.08

Table 25. Statistical results for the winter MODIS 5-year moving average Snow Area for all basins

<i>DJF</i>	<i>North</i>	<i>South</i>	<i>East</i>	<i>West</i>	<i>NorthWest</i>	<i>NorthEast</i>	<i>SouthWest</i>	<i>SouthEast</i>	<i>WestWest</i>	<i>WestEast</i>	<i>EastWest</i>	<i>EastEast</i>
<i>Slope</i>	-17.41	-12.15	-15.93	-13.63	-9.50	-7.91	-4.13	-8.02	-8.12	-5.51	-4.07	-11.86
<i>St. error of the slope</i>	9.17	9.70	12.83	7.75	4.88	5.61	2.95	7.33	4.77	3.25	4.55	8.39
<i>R²</i>	0.20	0.10	0.10	0.18	0.21	0.12	0.12	0.08	0.17	0.17	0.05	0.12
<i>F statistics</i>	3.61	1.57	1.54	3.09	3.79	1.99	1.96	1.20	2.89	2.88	0.80	2.00
<i>Regression sum of squares</i>	103112.50	50201.33	86317.91	63186.27	30708.79	21278.68	5795.71	21882.39	22419.01	10330.49	5631.04	47855.43
<i>Intercept</i>	35054.25	24475.20	32089.73	27439.71	19130.21	15924.04	8309.50	16165.69	16346.11	11093.60	8195.94	23893.79
<i>St. error of the intercept</i>	18440.88	19515.41	25810.43	15595.57	9820.03	11278.14	5928.61	14739.65	9600.61	6536.89	9144.45	16884.54
<i>St. error of the Y</i>	169.04	178.89	236.60	142.96	90.02	103.38	54.35	135.12	88.01	59.92	83.83	154.78
<i>Degrees of freedom</i>	14.00	14.00	14.00	14.00	14.00	14.00	14.00	14.00	14.00	14.00	14.00	14.00
<i>Residual sum of squares</i>	400062.42	448043.26	783709.21	286132.56	113446.20	149637.29	41349.57	255587.03	108433.14	50269.80	98373.93	335384.61

Table 26. Statistical results for the spring MODIS 5-year moving average Snow Area for all basins

<i>MAM</i>	<i>North</i>	<i>South</i>	<i>East</i>	<i>West</i>	<i>NorthWest</i>	<i>NorthEast</i>	<i>SouthWest</i>	<i>SouthEast</i>	<i>WestWest</i>	<i>WestEast</i>	<i>EastWest</i>	<i>EastEast</i>
<i>Slope</i>	-0.67	-0.17	1.54	-2.39	-1.85	1.17	-0.54	0.37	-1.89	-0.50	0.91	0.64
<i>St. error of the slope</i>	4.03	3.19	3.40	3.86	2.64	1.44	1.23	1.97	2.54	1.34	1.09	2.31
<i>R²</i>	0.00	0.00	0.01	0.03	0.03	0.05	0.01	0.00	0.04	0.01	0.05	0.01
<i>F statistics</i>	0.03	0.00	0.21	0.38	0.49	0.66	0.19	0.03	0.55	0.14	0.69	0.08
<i>Regression sum of squares</i>	154.60	10.16	805.67	1934.32	1157.63	467.34	99.14	45.94	1212.65	83.82	279.12	137.47
<i>Intercept</i>	1369.34	354.98	-3088.04	4809.68	3720.61	-2354.31	1089.05	-734.96	3807.65	1001.77	-1820.25	-1272.95
<i>St. error of the intercept</i>	8103.32	6415.10	6831.76	7762.72	5308.92	2896.47	2464.47	3967.51	5111.35	2698.70	2186.22	4650.92
<i>St. error of the Y</i>	74.28	58.81	62.63	71.16	48.67	26.55	22.59	36.37	46.85	24.74	20.04	42.63
<i>Degrees of freedom</i>	14.00	14.00	14.00	14.00	14.00	14.00	14.00	14.00	14.00	14.00	14.00	14.00
<i>Residual sum of squares</i>	77248.53	48414.08	54907.18	70891.27	33157.07	9869.64	7145.18	18518.26	30735.19	8567.86	5622.78	25447.30

Table 27. Statistical results for the summer MODIS 5-year moving average Snow Area for all basins

<i>JJA</i>	<i>North</i>	<i>South</i>	<i>East</i>	<i>West</i>	<i>NorthWest</i>	<i>NorthEast</i>	<i>SouthWest</i>	<i>SouthEast</i>	<i>WestWest</i>	<i>WestEast</i>	<i>EastWest</i>	<i>EastEast</i>
<i>Slope</i>	0.01	0.00	0.00	0.01	0.01	0	0	0	0.01	0	0	0
<i>St. error of the slope</i>	0.01	0.00	0.00	0.01	0.01	0	0	0	0.01	0	0	0
<i>R²</i>	0.17	0.14	0.56	0.17	0.17	1.00	0.18	0.56	0.18	0.65	1.00	1.00
<i>F statistics</i>	2.95	2.26	18.16	2.96	2.95	-	2.99	18.16	2.98	25.67	-	-
<i>Regression sum of squares</i>	0.03	0.00	0.00	0.05	0.03	0	0.00	0.00	0.05	0	0	0
<i>Intercept</i>	-18.59	-4.76	0.63	-23.98	-18.59	0	-5.39	0.63	-24.07	0.09	0	0
<i>St. error of the intercept</i>	10.78	3.15	0.15	13.88	10.78	0	3.11	0.15	13.88	0.02	0	0
<i>St. error of the Y</i>	0.10	0.03	0.00	0.13	0.10	0	0.03	0.00	0.13	0	0	0
<i>Degrees of freedom</i>	14.00	14.00	14.00	14.00	14.00	14.00	14.00	14.00	14.00	14.00	14.00	14.00
<i>Residual sum of squares</i>	0.14	0.01	0.00	0.23	0.14	0	0.01	0	0.23	0	0	0

Table 28. Statistical results for the fall MODIS 5-year moving average Snow Area for all basins

<i>SON</i>	<i>North</i>	<i>South</i>	<i>East</i>	<i>West</i>	<i>NorthWest</i>	<i>NorthEast</i>	<i>SouthWest</i>	<i>SouthEast</i>	<i>WestWest</i>	<i>WestEast</i>	<i>EastWest</i>	<i>EastEast</i>
<i>Slope</i>	-6.33	-3.28	-1.95	-4.42	-3.46	-2.88	-0.96	-2.32	-2.44	-1.98	-2.01	-3.19
<i>St. error of the slope</i>	0.99	0.50	0.27	0.67	0.55	0.48	0.13	0.40	0.39	0.32	0.33	0.55
<i>R²</i>	0.74	0.75	0.79	0.76	0.74	0.72	0.81	0.71	0.74	0.73	0.72	0.70
<i>F statistics</i>	40.70	42.70	51.70	43.33	39.14	35.36	58.06	33.57	39.67	37.75	36.33	33.40
<i>Regression sum of squares</i>	13640.49	3667.29	1297.65	6637.67	4062.02	2815.21	314.63	1833.57	2024.89	1330.29	1375.23	3456.81
<i>Intercept</i>	12744.72	6608.37	3930.96	8890.55	6954.88	5789.85	1935.67	4672.69	4910.60	3979.95	4046.80	6415.74
<i>St. error of the intercept</i>	1997.05	1011.01	546.51	1350.24	1111.26	973.40	253.94	806.23	779.41	647.56	671.16	1109.84
<i>St. error of the Y</i>	18.31	9.27	5.01	12.38	10.19	8.92	2.33	7.39	7.14	5.94	6.15	10.17
<i>Degrees of freedom</i>	14.00	14.00	14.00	14.00	14.00	14.00	14.00	14.00	14.00	14.00	14.00	14.00
<i>Residual sum of squares</i>	4691.83	1202.48	351.36	2144.80	1452.78	1114.67	75.86	764.69	714.66	493.32	529.92	1449.06

APPENDIX II

SNOW COVER DAYS

Table 29. MODIS annual snow cover days

<i>Year</i>	<i>NORTH</i>	<i>SOUTH</i>	<i>WEST</i>	<i>EAST</i>	<i>NORTHWEST</i>	<i>NORTHEAST</i>	<i>SOUTHWEST</i>	<i>SOUTHEAST</i>	<i>WESTWEST</i>	<i>WESTEAST</i>	<i>EASTWEST</i>	<i>EASTEAST</i>
2001	201	201	201	148	201	148	201	148	201	201	148	148
2002	204	168	204	158	204	152	168	158	204	185	153	158
2003	200	205	200	182	200	156	200	182	200	200	177	169
2004	198	198	198	151	198	151	198	151	198	198	151	151
2005	216	203	216	198	216	198	203	157	216	216	157	157
2006	200	188	200	129	200	129	188	129	200	190	129	129
2007	169	163	169	155	169	148	163	155	169	169	148	155
2008	175	175	175	126	175	105	175	126	175	175	111	126
2009	204	204	204	150	204	150	204	150	204	198	150	150
2010	149	149	149	102	149	89	149	102	149	149	89	102
2011	202	202	202	177	202	177	202	177	202	191	177	177
2012	193	193	193	153	193	148	193	153	193	193	153	153
2013	185	185	185	162	185	152	185	162	185	174	152	162
2014	171	145	171	115	171	109	145	115	171	160	109	115
2015	188	171	188	147	188	147	171	147	188	188	147	147
2016	144	144	144	136	144	134	144	136	144	139	134	136
2017	172	172	172	132	172	127	172	132	172	165	127	132
2018	182	182	182	137	182	114	182	134	182	182	86	134

Table 30. Landsat annual snow cover days

<i>Year</i>	<i>North</i>	<i>South</i>	<i>West</i>	<i>East</i>	<i>NorthWest</i>	<i>NorthEast</i>	<i>SouthWest</i>	<i>SouthEast</i>	<i>WestWest</i>	<i>WestEast</i>	<i>EastWest</i>	<i>EastEast</i>
1985	255	210	255	210	255	209	210	210	255	255	210	210
1986	269	267	269	252	269	220	266	250	269	269	220	252
1987	285	285	285	281	285	200	285	281	285	285	200	281
1988	276	256	276	256	276	224	256	256	276	276	208	256
1989	255	255	255	197	255	164	255	197	255	255	164	197
1990	260	228	260	228	260	140	228	228	260	260	140	228
1991	272	272	272	271	272	231	272	271	272	272	231	271
1992	285	293	289	288	285	248	289	288	289	289	232	288
1993	287	287	287	287	287	239	287	287	287	287	207	287
1994	259	259	259	243	259	163	259	243	259	259	163	243
1995	275	275	275	275	275	227	275	275	275	275	179	275
1996	285	285	285	269	285	237	285	269	285	285	237	269
1997	279	272	279	256	279	183	243	256	279	279	179	256
1998	275	227	275	227	275	179	227	227	275	275	147	227
1999	239	214	239	214	239	173	214	214	239	239	173	214
2000	301	295	301	284	301	152	262	284	301	301	152	284
2001	281	253	281	216	281	216	253	216	280	281	160	216
2002	268	267	268	259	268	187	267	259	268	268	226	259
2003	268	278	268	278	268	251	268	278	268	268	251	278
2004	260	260	260	255	260	246	260	255	260	260	214	255
2005	295	281	295	234	295	151	281	234	295	295	150	234
2006	281	282	282	205	281	148	281	205	282	282	148	205
2007	227	227	227	211	227	179	227	195	227	227	163	211
2008	277	261	277	244	277	172	261	244	277	277	172	244
2009	268	268	268	268	268	196	268	268	268	268	196	268
2010	246	246	246	229	246	221	246	181	246	246	110	229
2011	270	270	270	268	270	212	270	268	270	270	173	268
2012	288	272	288	272	288	272	272	269	288	288	272	269
2013	268	247	268	231	268	151	247	231	267	266	199	231
2014	289	244	289	240	289	239	244	168	289	289	129	239
2015	261	261	261	228	261	172	261	228	261	261	172	228
2016	249	249	249	193	249	153	249	193	249	249	153	193
2017	278	263	278	231	278	140	263	231	278	278	140	231
2018	277	164	277	148	277	94	164	148	277	259	94	148

REFERENCES

- Akyürek, Z., & Tekeli, A. (2006). Commentary on comparison of MODIS snow cover and albedo products with ground observations over the mountainous terrain of Turkey. *Hydrology and Earth System Sciences Discussions*, 3(6), 3655-3673.
- Aouad-Rizk, A., Job, J.-O., Khalil, S., Touma, T., Bitar, C., Boquillon, C., & Najem, W. (2005). Snow in Lebanon: a preliminary study of snow cover over Mount Lebanon and a simple snowmelt model/Etude préliminaire du couvert neigeux et modèle de fonte des neige pour le Mont Liban. *Hydrological sciences journal*, 50(3).
- Bourdelles, B., & Fily, M. (1993). Snow grain-size determination from Landsat imagery over Terre Adelie, Antarctica. *Annals of glaciology*, 17, 86-92.
- Chang, A., Foster, J., & Hall, D. K. (1987). Nimbus-7 SMMR derived global snow cover parameters. *Annals of glaciology*, 9, 39-44.
- Chang, A., Foster, J., Kelly, R., Josberger, E., Armstrong, R., & Mognard, N. (2005). Analysis of ground-measured and passive-microwave-derived snow depth variations in midwinter across the northern Great Plains. *Journal of Hydrometeorology*, 6(1), 20-33.
- Cline, D., Elder, K., & Bales, R. (1998). Scale effects in a distributed snow water equivalence and snowmelt model for mountain basins. *Hydrological Processes*, 12(10-11), 1527-1536.
- Cook, B. I., Anchukaitis, K. J., Touchan, R., Meko, D. M., & Cook, E. R. (2016). Spatiotemporal drought variability in the Mediterranean over the last 900 years. *Journal of Geophysical Research: Atmospheres*, 121(5), 2060-2074.
- Deems, J. S., Painter, T. H., & Finnegan, D. C. (2013). Lidar measurement of snow depth: a review. *J. Glaciol*, 59(215), 467-479.
- Derksen, C. (2008). The contribution of AMSR-E 18.7 and 10.7 GHz measurements to improved boreal forest snow water equivalent retrievals. *Remote Sensing of Environment*, 112(5), 2701-2710.
- Derksen, C., Walker, A., & Goodison, B. (2005). Evaluation of passive microwave snow water equivalent retrievals across the boreal forest/tundra transition of western Canada. *Remote Sensing of Environment*, 96(3-4), 315-327.
- Dietz, A. J., Kuenzer, C., Gessner, U., & Dech, S. (2012). Remote sensing of snow—a review of available methods. *International Journal of Remote Sensing*, 33(13), 4094-4134.

- Dozier, J. (1987). *Remote sensing of snow characteristics in the southern Sierra Nevada*. Paper presented at the Proceedings of the Vancouver Symposium on Large Scale Effects of Seasonal Snow Cover. IAHS Publication.
- Dozier, J. (1989). Spectral signature of alpine snow cover from the Landsat Thematic Mapper. *Remote Sensing of Environment*, 28, 9-22.
- Dozier, J., Bair, E. H., & Davis, R. E. (2016). Estimating the spatial distribution of snow water equivalent in the world's mountains. *Wiley Interdisciplinary Reviews: Water*, 3(3), 461-474.
- Dozier, J., & Painter, T. H. (2004). Multispectral and hyperspectral remote sensing of alpine snow properties. *Annu. Rev. Earth Planet. Sci.*, 32, 465-494.
- Fayad, A., Gascoin, S., Faour, G., Fanise, P., Drapeau, L., Somma, J., . . . Escadafal, R. (2017). Snow observations in Mount Lebanon (2011–2016). *Earth System Science Data*, 9(2).
- Fayad, A., Gascoin, S., Faour, G., López-Moreno, J. I., Drapeau, L., Le Page, M., & Escadafal, R. (2017). Snow hydrology in Mediterranean mountain regions: A review. *Journal of hydrology*, 551, 374-396.
- Fily, M., Bourdelles, B., Dedieu, J., & Sergent, C. (1997). Comparison of in situ and Landsat Thematic Mapper derived snow grain characteristics in the Alps. *Remote Sensing of Environment*, 59(3), 452-460.
- Foster, J., Hall, D., Kelly, R., & Chiu, L. (2009). Seasonal snow extent and snow mass in South America using SMMR and SSM/I passive microwave data (1979–2006). *Remote Sensing of Environment*, 113(2), 291-305.
- Frei, A., Tedesco, M., Lee, S., Foster, J., Hall, D. K., Kelly, R., & Robinson, D. A. (2012). A review of global satellite-derived snow products. *Advances in Space Research*, 50(8), 1007-1029.
- Giorgi, F., & Lionello, P. (2008). Climate change projections for the Mediterranean region. *Global and planetary change*, 63(2-3), 90-104.
- Gorelick, N., Hancher, M., Dixon, M., Ilyushchenko, S., Thau, D., & Moore, R. (2017). Google Earth Engine: Planetary-scale geospatial analysis for everyone. *Remote Sensing of Environment*, 202, 18-27.
- Goulden, M. L., & Bales, R. C. (2014). Mountain runoff vulnerability to increased evapotranspiration with vegetation expansion. *Proceedings of the National Academy of Sciences*, 111(39), 14071-14075.
- Grayson, R. B. (1996). *Hydrological recipes: estimation techniques in Australian hydrology*: Cooperative Research Centre for Catchment Hydrology.

- Hall, D. K., Riggs, G. A., Salomonson, V. V., DiGirolamo, N. E., & Bayr, K. J. (2002). MODIS snow-cover products. *Remote Sensing of Environment*, 83(1-2), 181-194.
- Hijmans, R. J., & van Etten, J. (2014). raster: Geographic data analysis and modeling. *R package version*, 2(8).
- Hill, D. F., Burakowski, E. A., Crumley, R. L., Keon, J., Hu, J. M., Arendt, A. A., . . . Wolken, G. J. (2019). Converting snow depth to snow water equivalent using climatological variables. *The Cryosphere*, 13(7), 1767-1784.
- Hüsler, F., Jonas, T., Riffler, M., Musial, J. P., & Wunderle, S. (2014). A satellite-based snow cover climatology (1985–2011) for the European Alps derived from AVHRR data. *The Cryosphere*, 8(1), 73-90.
- Jaafar, H., Ahmad, F., Holtmeier, L., & King-Okumu, C. (2019). Refugees, water balance, and water stress: Lessons learned from Lebanon. *Ambio*, 1-15.
- Jonas, T., Marty, C., & Magnusson, J. (2009). Estimating the snow water equivalent from snow depth measurements in the Swiss Alps. *Journal of hydrology*, 378(1-2), 161-167.
- Kelley, C. P., Mohtadi, S., Cane, M. A., Seager, R., & Kushnir, Y. (2015). Climate change in the Fertile Crescent and implications of the recent Syrian drought. *Proceedings of the National Academy of Sciences*, 112(11), 3241-3246.
- Knowles, N., Dettinger, M. D., & Cayan, D. R. (2006). Trends in snowfall versus rainfall in the western United States. *Journal of Climate*, 19(18), 4545-4559.
- Kundzewicz, Z., & Robson, A. (2000). Detecting trend and other changes in hydrological data. World Climate Program–Water, WMO. *UNESCO, WCDMP-45, WMO/TD, 1013*, 157.
- Leroux, C., Deuzé, J. L., Goloub, P., Sergent, C., & Fily, M. (1998). Ground measurements of the polarized bidirectional reflectance of snow in the near-infrared spectral domain: Comparisons with model results. *Journal of Geophysical Research: Atmospheres*, 103(D16), 19721-19731.
- Lichtenegger, J., Seidel, K., Keller, M., & Haefner, H. (1981). Snow surface measurements from digital Landsat MSS data. *Hydrology Research*, 12(4-5), 275-288.
- Lievens, H., Demuzere, M., Marshall, H.-P., Reichle, R. H., Brucker, L., Brangers, I., . . . Immerzeel, W. W. (2019). Snow depth variability in the Northern Hemisphere mountains observed from space. *Nature communications*, 10(1), 1-12.
- Liu, J., Woodcock, C. E., Melloh, R. A., Davis, R. E., McKenzie, C., & Painter, T. H. (2008). Modeling the view angle dependence of gap fractions in forest canopies:

- Implications for mapping fractional snow cover using optical remote sensing. *Journal of Hydrometeorology*, 9(5), 1005-1019.
- Margane, A., Schuler, P., Königer, P., Abi Rizk, J., Stoeckl, L., & Raad, R. (2013). *Hydrogeology of the Groundwater Contribution Zone of Jeita Spring. Technical Cooperation Project Protection of Jeita Spring*. Retrieved from
- Maurer, E. P., Stewart, I., Bonfils, C., Duffy, P. B., & Cayan, D. (2007). Detection, attribution, and sensitivity of trends toward earlier streamflow in the Sierra Nevada. *Journal of Geophysical Research: Atmospheres*, 112(D11).
- Mhaweij, M., Faour, G., Fayad, A., & Shaban, A. (2014). Towards an enhanced method to map snow cover areas and derive snow-water equivalent in Lebanon. *Journal of hydrology*, 513, 274-282.
- Morán-Tejeda, E., Lorenzo-Lacruz, J., López-Moreno, J. I., Rahman, K., & Beniston, M. (2014). Streamflow timing of mountain rivers in Spain: recent changes and future projections. *Journal of hydrology*, 517, 1114-1127.
- Olmedo, G., Ortega-Farias, S., Fonseca-Luengo, D., de la Fuente-Saiz, D., & Fuentes-Peñailillo, F. (2017). Water: actual evapotranspiration with energy balance models. *R Package Version 0.6*.
- Painter, T. H., Dozier, J., Roberts, D. A., Davis, R. E., & Green, R. O. (2003). Retrieval of subpixel snow-covered area and grain size from imaging spectrometer data. *Remote Sensing of Environment*, 85(1), 64-77.
- Painter, T. H., Rittger, K., McKenzie, C., Slaughter, P., Davis, R. E., & Dozier, J. (2009). Retrieval of subpixel snow covered area, grain size, and albedo from MODIS. *Remote Sensing of Environment*, 113(4), 868-879.
- Rosenthal, W., & Dozier, J. (1996). Automated mapping of montane snow cover at subpixel resolution from the Landsat Thematic Mapper. *Water Resources Research*, 32(1), 115-130.
- Scherer, D., Hall, D. K., Hochschild, V., König, M., Winther, J. g., Duguay, C. R., . . . Seidel, K. (2005). Remote sensing of snow cover. *GEOPHYSICAL MONOGRAPH-AMERICAN GEOPHYSICAL UNION*, 163, 7.
- Seidel, K., & Martinec, J. (2004). *Remote sensing in snow hydrology: runoff modelling, effect of climate change*: Springer Science & Business Media.
- Selkowitz, D. J., & Forster, R. R. (2016). Automated mapping of persistent ice and snow cover across the western US with Landsat. *ISPRS Journal of Photogrammetry and Remote Sensing*, 117, 126-140.
- Shaban, A., Faour, G., Khawlie, M., & Abdallah, C. (2004). Remote sensing application to estimate the volume of water in the form of snow on Mount

Lebanon/Application de la télédétection à l'estimation du volume d'eau sous forme de neige sur le Mont Liban. *Hydrological sciences journal*, 49(4).

Srivastava, P., Pandey, V., Suman, S., Gupta, M., & Islam, T. (2016). Available data sets and satellites for terrestrial soil moisture estimation *Satellite Soil Moisture Retrieval* (pp. 29-44): Elsevier.

Staenz, K., & Haefner, H. (1981). Spectral reflectance properties of snow in the Landsat MSS bands. *Canadian Journal of Remote Sensing*, 7(1), 41-50.

Tasumi, M., Allen, R. G., & Trezza, R. (2008). At-surface reflectance and albedo from satellite for operational calculation of land surface energy balance. *Journal of hydrologic engineering*, 13(2), 51-63.

Tong, J., Déry, S. J., Jackson, P. L., & Derksen, C. (2010). Snow distribution from SSM/I and its relationships to the hydroclimatology of the Mackenzie River Basin, Canada. *Advances in water resources*, 33(6), 667-677.

Vogel, S. W. (2002). Usage of high-resolution Landsat 7 band 8 for single-band snow-cover classification. *Annals of glaciology*, 34, 53-57.